ABSTRACT

RONG HUANG. The Effect of Electrospun Interlayers on the Delamination Resistance of Carbon Fiber Reinforced Epoxy. (Under the direction of Dr. Ericka Ford and Dr. Abdel-Fattah M. Seyam.)

Because of their high strength and stiffness, carbon fiber reinforced plastics (CFRP) are widely used engineering materials for construction and aerospace applications. Delamination within laminated CFRPs results in the complete failure of the composite, because it weakens the composite's strength through its thickness. Poor interfacial adhesion between carbon fibers and brittle matrix resin lead to delamination. In this research, the nanofibrous interlayers of polyvinyl alcohol (PVA) and polyvinyl acetate (PVAc) were studied as toughening agents within CFRPs.

In this thesis, the results and discussion section was divided into two parts. Part I discussed the effects of electrospinning parameters on web structure. Polymer type (PVA and PVAc) and concentration, tip-to-collector distance (TCD), and winding velocity of collected nanofibers were varied to explore their influence on fiber diameter, orientation distribution and morphology. Electrospun PVA, having a 12 cm TCD and 12% polymer concentration, presented the best measurements of fiber orientation- where the anisotropy ratio was 0.41.

Part II reported a study of CFRP toughening as a result of having electrospun PVA and PVAc interleaves within the composite. Electrospun PVAc toughened CFRPs the best. Composite samples containing electrospun PVAc interlayers resisted higher amounts of mechanical deformation. The optimal basis weight for PVAc nanofibers was 10 g/m^2,

where the toughness was improved by 25% without reducing the maximum shear strain and shear stress.

The Effect of Electrospun Interlayers on the Delamination Resistance of Carbon Fiber Reinforced Epoxy

by

Rong Huang

A thesis submitted to the graduate faculty of
North Carolina State University
in partial fulfillment of the
requirements for the degree of
Master of Science

Textile Engineering

Raleigh, North Carolina

2017

APPROVED BY

Dr. Abdel-Fattah Seyam	Dr. Mohamed Bourham
Co-chair	

Dr. Ericka Ford

Co-chair

DEDICATION

Dedicated to

The best parents in the world,

Hongmei Qiu & Weidong Huang

BIOGRAPHY

Rong Huang was born in 1994 in a small town in Taizhou city, Jiangsu Province, China. In May 2015, she received the Bachelor's Degree of Engineering in Nonwoven Material & Technology from Zhejiang Sci-Tech University, which was the first turning point in her life. Here, not only did she find some life-long time friends, but also learned to strive for everything she dreamt of. When she was an undergraduate student in Zheijang Sci-Tech University, she caught the chance to pursue her last semester abroad in College of Textiles in North Carolina University as a 3+X student, which was the second turning point.

It is difficult to survive abroad at the very beginning, but if you are dedicated and diligent, then nothing is impossible. Where there is a will, there is always a way.

She became more mature- being equipped with good personal qualities that are right for this age. Now in October 2017, she is qualified to be a master student, having a deep interest in electrospinning and carbon fiber reinforced plastics. Moreover, she has prepared herself to enter the Ph.D. program, which must be the third turning point in life. Tracking her experience, you can know her growth.

ACKNOWLEDGMENTS

The master thesis is a long journey that I could not accomplish without the help of many people. First and most importantly: Sincere thanks to my advisors Dr. Ericka Ford and Dr. Abdel-Fattah Seyam and my committee member Dr. Mohamed Bourham. They were ready all the time to guide and encourage me to overcome every challenge. All the members in my research group are creative and hard working. They always put forth helpful comments during our meetings and were patient while giving suggestions.

Here, especially, I want to say thanks to my parents and my dear friends. They never blame me for my faults, but were always patient in giving me advice and they supported me. The thesis is not the only qualifier towards to the master's degree- another is my response to all the people who care about me.

TABLE OF CONTENTS

LIST OF TABLES viii

LIST OF FIGURES ix

LIST OF APPENDIXES xii

LIST OF ABBREVIATIONS xiii

CHAPTER 1 INTRODUCTION 1

References 4

CHAPTER 2 LITERATURE REVIEW 7

2.1 Carbon Fiber Reinforced Plastics (CFRP) 7

2.1.1 Introduction to CFRPs 7

2.1.2 Carbon Fiber 8

2.1.2.1 The Structure of Carbon Fiber 8

2.1.2.2 Precursor of Carbon Fiber 10

2.1.2.3 Carbon Fiber Architecture 12

2.1.3 CFRP Matrix Resins 15

2.1.4 Delamination of CFRP 16

2.1.4.1 The Description of CFRP Delamination 16

2.1.4.2 Previous Work to Decrease Delamination 18

2.1.4.3 Nano-interleaves to Toughen Matrix Resin 20

2.1.5 Summaries and Conclusions 27

2.2 Electrospun Nanofibers 28
2.2.1 Introduction to Electrospinning 28
2.2.2 Electrospinning Process 28
2.2.3 Characterization of Nanoweb Structure 30
2.2.4 Electrospinning Parameters 31
2.2.5 The Effect of Electrospinning Parameters on Fiber Diameter 31
2.2.6 Fiber Diameter Distribution of Electrospun Fibers 35
2.2.7 Orientation of Electrospun Fibers 36
2.2.8 Morphology of Electrospun Fibers 37
2.2.9 Summaries and Conclusions 39
References 40
CHAPTER 3 EXPERIMENTS 48
3.1 Electrospinning 48
3.1.1 Raw Materials 48
3.1.2 Dope Preparation 48
3.1.3 Electrospinning Process 48
3.1.4 Scanning Electron Microscope (SEM) 50
3.1.5 Diameter Measurement by ImageJ 50
3.1.6 Fiber Orientation Characterized by MATLAB 50
3.2 Carbon Fiber Reinforced Plastics (CFRP) 51

3.2.1 Fabrication of CFRPs with Electrospun Interlayers 51

3.2.2 Interlaminar Shear Test 52

3.2.3 Characterization of Fracture Surface by Confocal Microscope 53

References 54

APPENDIX A.Customized Code to Characterize the Orientation of Fibers [2] 55

CHAPTER 4 RESULTS AND DISCUSSIONS 58

4.1 The Effect of Electrospinning Parameters on web structure 58

4.1.1 The Effect of Concentration 58

4.1.2 The Effect of Collector Surface Velocity 60

4.1.3 The Effect of the Tip to Collector Distance 63

4.1.4 Summaries and Conclusions 65

4.1.5 Preliminary Experiment 66

4.1.5.1 Design of Test Sample 66

4.1.5.2 Decision of Composites Layers 67

4.1.6 The Effect of Electrospun Interlayers on the CFRP Delamination Resistance 70

4.1.7 Morphology of Fracture Surface 72

4.1.8 Summaries and Conclusions 74

References 76

APPENDIX B.Calculation of PVAc Volume 78

LIST OF TABLES

Table 2.1 The mechanical properties of common fibers in fiber reinforced plastics [1] 8

Table 3.1 Summary for electrospinning materials 48

Table 3.2 The Specification of Carbon Fabric 51

Table 4.1 Electrospinning parameters of first trial of eletrospun PVA 58

Table 4.2 Optimized electrospinning parameters for electrospun PVA 58

Table 4.3 Plan of electrospinning parameters to study the effect of drum surface speed on web structure 61

Table 4.4 Plan of electrospinning parameters to study the effect of TCD on web structure 63

Table 4.5 Electrospinning parameters for the electrospun interleaves in the CFRP 70

Table 4.6 The summary of shear test 71

LIST OF FIGURES

Figure 2.1 The anisotropic structure of graphite [3] 9

Figure 2.2 The turbostratic structure of graphite [3][4]. On the left is the schematic of carbon fiber structure, and right is one layer of bended graphite crystal structure 10

Figure 2.3 Three types of processes for fabrication of carbon fibers [1] 11

Figure 2.4 Thermal degradation of rayon to carbon 12

Figure 2.5 Three fiber architectures with continuous fibers. (a) unidirectional, (b) two-dimensional, (c)three-dimensional [11] 13

Figure 2.6 Basis weave pattern [3] 14

Figure 2.7 3D woven structure. Thin and open (left) & thick and tight (right). 15

Figure 2.8 Thermoplastic and thermosetting matrix resins [12] 16

Figure 2.9 Scheme of damage mode in CFRP [14]: 17

Figure 2.10 Illustration of the fracture behavior in response to tensile loading [15] 18

Figure 2.11 SEM images taken from the ENF test sample edges: (A) without interleaf, and (B) with an interleaf, where (a) general rack propagation pattern, (b) enlarged view of (a) and (c) SEM images of the upper and (d) lower edges. 22

Figure 2.12 SEM images of the fracture surface of ENF test specimen with and without interleaves taken at low and high magnifications. [15] 23

Figure 2.13 SEM images of the fracture surface of DCB test specimen with and without interleaves. [24] 24

Figure 2.14 SEM images of fracture surface under DCB test. (a) control sample, (b-d) samples toughened by PCL nanofibers with concentration from 12 wt %, 15 wt %, 20 wt %, (e, f) samples toughened by PVDF and PAN [9]..... 26
Figure 2.15 Optical micrograph of thermoplastic/epoxy blends before (top) and after curing (bottom). 27
Figure 2.16 Electrospinning setup with horizontal collector in laboratory scale [37]..... 29
Figure 2.17 Collectors of the conductive plate (left) and rotating drum (right) [57][58] 37
Figure 2.18 Optical microscope images with the increase of PS concentration. 38
Figure 3.1 Electrospinning equipment with rotating drum 49
Figure 3.2 Scheme of electrospinning set up with rotating drum 49
Figure 3.3 Tool interface of ImageJ 50
Figure 3.4 Fabrication of CFRP with the vacuum assisted resin transfer modeling in the laboratory scale 52
Figure 3.5 Schematic diagrams of CFRP fabrication with the vacuum assisted resin transfer modeling [3] 52
Figure 3.6 MTS Landmark Servohydraulic Test Systems available in the Composite Core Facility, College of Textiles, NC State University. 53
Figure 3.7 Olympus LEXT 4000 confocal microscopy available in the Chemistry Lab, College of Textiles, NC State University. 53
Figure 4.1 SEM images at 5k of electrospun PVA with the first trail electrospinning parameters (left) and with optimized electrospinning parameters (right) 58
Figure 4.2 SEM images at 5k for PVAc with different concentration..... 59

Figure 4.3 Effect of concentration on PVAc fiber diameter 60
Figure 4.4 SEM images at 25k and fiber diameter distribution histograms with the fiber diameter displayed on the top right corner 61
Figure 4.5 SEM images at 5k and fiber orientation distribution histograms with the Ht values displayed on the top right corner 62
Figure 4.6 The effect of TCD on fiber diameter 63
Figure 4.7 The effect of TCD on fiber orientation 64
Figure 4.8 SEM images of electrospun PVAc at 1k with different TCD 65
Figure 4.9 Designs of fabrication of CFRP for interlaminar shear test in the cross section 67
Figure 4.10 Fabrication of sample for interlaminar shear test with specific size 67
Figure 4.11 The results for interlaminar shear test with 2-layer composites 68
Figure 4.12 CFRP sample manufacture with 8 layers (4 layers each side) with two extra cushions each side. From the top to the bottom are top and left views as well as the schematic of final sample manufacture 70
Figure 4.13 Graph of shear test results with different eletrospun interlayer with x axis as shear strain and the y axis as shear stress 72
Figure 4.14 The toughness of CFRP with different electrospun interlayers 72
Figure 4.15 Fracture surface images taken from confocal microscopy. From the top to the bottom are fracture surface of control sample, CFRP with electrospun PVA and PVAc interleaves with basis weight as 4 g/m^2. Left: magnification as 5, 2D image. Right: magnification as 100, 3D image. 73

LIST OF APPENDIXES

APPENDIX A.Customized Code to Characterize the Orientation of Fibers [2] 55

APPENDIX B.Calculation of PVAc Volume..... 78

LIST OF ABBREVIATIONS

CFRP	Carbon Fiber Reinforced Plastic
PVA	Polyvinyl Alcohol
PVAc	Polyvinyl Acetate
VARTM	Vacuum Assisted Resin Transfer Modeling
PEEK	Polyether Ether Ketone
PCL	Polycaprolactone
PAN	Polyacrylonitrile
PA	Polyamide
PA 6,6	Polyamide 6,6
PVDF	Polyvinylidene Fluoride
PSF	Polysulfone
PC	Polycarbonate

CHAPTER 1 INTRODUCTION

Carbon fiber reinforced plastics (CFRPs) have wide applications in aerospace, construction, transportation and the military, which are due to their high specific strength and specific stiffness [1]. These uses are mostly attributed to the extraordinary performance of the carbon fiber, which acts to mechanically reinforce composites. The unique graphitic crystal structure comprises packed sheets of carbon that are covalently bonded in-plane, but in the transverse direction sheets are linked by weak Van der Waals forces [2][3]. Although the mechanical properties along the carbon fiber axis are excellent, low performance is exhibited along the though-thickness direction. Low performance such as weak loop strength and shear strength are observed. To take advantage of carbon fiber reinforcement in the CFRP, the effectiveness of load transfer between fiber and matrix resin cannot be ignored. Because the strength and stiffness of matrix resin is incompatible with carbon fiber layers, the compression strength is dominated by weak matrix polymer, which is less resistant to load than carbon fiber.

Delamination is one of several major failure modes among CFRPs. It results from poor interfacial adhesion between the inert carbon fibers and matrix resin- which is relatively more brittle. Many approaches have been studied to resolve this problem. Most efforts are based on improving interfacial adhesion between carbon fiber and matrix resin, increasing though-thickness strength, and enhancing the toughness of matrix resins. The introduction of nanofibers as a secondary reinforcement layer- at the interface of carbon fiber and matrix resin- has been shown to be a viable toughening mechanism among composites. CFRP interleaves are nanoscale fibers that are light weight, have high surface

area, are porous, and have high fiber aspect ratios. Having high surface area and porosity makes nanofibers amendable to good adhesion between those nanofibers and matrix resin.

Electrospinning is the straightforward, convenient and inexpensive method of controlling nanofiber diameter and morphology during fabrication [5]. The final nanofibrous web structure is dictated by the polymer solution (i.e. dope), processing, and ambient parameters; each plays a crucial role in affecting CFRP toughening [6][7]. Many polymers have been used as electrospun interleaves for the ultimate goal of enhancing CFRP toughness: poly caprolactone (PCL) [8], polyacrylonitrile (PAN) [9][15], polyamide (PA) [10], polyamide 6,6 (PA 6,6) [11][14], polyvinylidene fluoride (PVDF) [12], polysulfone (PSF) [13], and polytherketone cardo (PEK-C) [6] to name a few.

In this work, polyvinyl alcohol (PVA) and polyvinyl acetate (PVAc) were selected to electrospin interleaves for CFRPs. There is limited literature [4] [16] [17] available on electrospun PVA interleaves; however, no work is done on PVAc interleaves until reported in this thesis- to the author's knowledge. This research has investigated the potential of electrospun PVA and PVAc to enhance the delamination toughness of CFRPs. Both PVA and PVAc are vinyl polymers that have a pendant hydroxyl group and acetate group, respectively. Differences between these side groups affect their chemistry; PVA is hydrophilic and water soluble, while PVAc is hydrophobic and soluble in acetic acid.

PVA is produced by the hydrolysis (or alcoholysis) of PVAc. PVAc hydrolysis is carried out to varying degrees: 88-99% are most common. The formation of inter- and intramolecular hydrogen bonding induces crystallization among PVA. Residual acetate groups can disrupt intermolecular hydrogen bonding and thus crystallization. Therefore, the degree of hydrolysis or content of residual acetate groups will influence polymer

chemistry, solubility, and crystallinity [19]. PVA is a nontoxic, inexpensive ($3-5/kg) semicrystalline polymer, having excellent mechanical properties (tensile strength values as high as 0.8-1.6 GPa and tensile modulus of 23-40 GPa have been reported), water solubility, and thermal resistance [18]. In comparison to PVA, the mechanical properties of PVAc (such as stiffness and strength) are much lower. This is due to its amorphous structure.

The Results & Discussion section is divided into two parts: Part I on the effect of electrospinning parameters on web structure and Part II on the effect of electrospun interleaves on the delamination resistance of carbon fiber reinforced epoxy.

In Part I, the following was studied:

1. Effect of varying electrospinning parameters (concentration, tip-to-collector distance and winder velocity for take-up) on PVA and PVAc web structure.
2. Characterization of electrospun web structure (including fiber shape, diameter distribution, and orientation).

In Part II, the following was studied:

1. Properties of electrospun interleaves that are desirable for CFRPs.
2. Fabrication of CFRPs with and without electrospun interleaves by vacuum assisted resin transfer molding (VARTM).
3. Characterization of CFRPs by lap shear testing and their morphology by confocal microscopy.

References

[1] Che, Demeng, et al. "Machining of carbon fiber reinforced plastics/polymers: A literature review." *Journal of Manufacturing Science and Engineering* 136.3 (2014): 034001.

[2] Soutis, C. "Carbon fiber reinforced plastics in aircraft construction." *Materials Science and Engineering: A* 412.1 (2005): 171-176.

[3] Fitzer, Erich, and Lalit M. Manocha. *Carbon reinforcements and carbon/carbon composites*. Springer Science & Business Media, 2012.

[4] Beylergil, Bertan, Metin TANOĞLU, and Engin AKTAŞ. "MODIFICATION OF CARBON FIBRE/EPOXY COMPOSITES BY POLYVINYL ALCO-HOL (PVA) BASED ELECTROSPUN NANOFIBRES." *Advanced Composites Letters* 25.3 (2016): 69-76.

[5] Yao, Li, et al. "Electrospinning and stabilization of fully hydrolyzed poly (vinyl alcohol) fibers." *Chemistry of Materials* 15.9 (2003): 1860-1864.

[6] Zhang, Jin, Tong Lin, and Xungai Wang. "Electrospun nanofibre toughened carbon/epoxy composites: Effects of polyetherketone cardo (PEK-C) nanofibre diameter and interlayer thickness." *Composites science and technology* 70.11 (2010): 1660-1666.

[7] Stahl, James J., Alexander E. Bogdanovich, and Philip D. Bradford. "Carbon nanotube shear-pressed sheet interleaves for Mode I interlaminar fracture toughness enhancement." *Composites Part A: Applied Science and Manufacturing* 80 (2016): 127-137.

[8] Saghafi, Hamed, et al. "The effect of interleaved composite nanofibrous mats on delamination behavior of polymeric composite materials." *Composite Structures* 109 (2014): 41-47.

[9] Zhang, Jin, et al. "Phase morphology of nanofibre interlayers: critical factor for toughening carbon/epoxy composites." *Composites science and technology* 72.2 (2012): 256-262.

[10] Daelemans, Lode, et al. "Nanofibre bridging as a toughening mechanism in carbon/epoxy composite laminates interleaved with electrospun polyamide nanofibrous veils." *Composites Science and Technology* 117 (2015): 244-256.

[11] Bovicelli, F., et al. "On consideration the mode I fracture response of CFRP composite interleaved by composite nanofibers." *Procedia Materials Science* 3 (2014): 1316-1321.

[12] Saghafi, H., et al. "Impact response of glass/epoxy laminate interleaved with nanofibrous mats." *Engineering Solid Mechanics* 1.3 (2013): 85-90.

[13] Li, Gang, et al. "Novel carbon fiber/epoxy composite toughened by electrospun polysulfone nanofibers." *Materials Letters* 62.3 (2008): 511-514.

[14] Palazzetti, Roberto, et al. "Influence of electrospun Nylon 6, 6 nanofibrous mats on the interlaminar properties of Gr–epoxy composite laminates." *Composite structures* 94.2 (2012): 571-579.

[15] Khan, Shafi Ullah, and Jang-Kyo Kim. "Improved interlaminar shear properties of multiscale carbon fiber composites with bucky paper interleaves made from carbon nanofibers." *Carbon* 50.14 (2012): 5265-5277.

[16] Phong, Nguyen Tien, et al. "Improvement in the mechanical performances of carbon fiber/epoxy composite with addition of nano-(polyvinyl alcohol) fibers." *Composite Structures* 99 (2013): 380-387.

[17] Shao, Yongzheng, et al. "Effect of physical modification of matrix by nano (polyvinyl alcohol) fibers on fatigue performance of carbon fiber fabric-reinforced vinylester composites." *Journal of Composite Materials* 50.29 (2016): 4065-4075.

[18] Park, Jong-Chul, et al. "Electrospun poly (vinyl alcohol) nanofibers: effects of degree of hydrolysis and enhanced water stability." *Polymer journal* 42.3 (2010): 273.

[19] Hassan, Christie M., and Nikolaos A. Peppas. "Structure and applications of poly (vinyl alcohol) hydrogels produced by conventional crosslinking or by freezing/thawing methods." *Biopolymers· PVA Hydrogels, Anionic Polymerisation Nanocomposites*. Springer Berlin Heidelberg, 2000. 37-65.

CHAPTER 2 LITERATURE REVIEW

2.1 Carbon Fiber Reinforced Plastics (CFRP)

2.1.1 Introduction to CFRPs

Composite manufacturing requires at least two different components. The choice of matrix polymer and reinforcement material is designed to meet the requirements of the application. These are popular engineering materials, having a wide variety of applications; such as in aerospace, construction, consumer products, and transportation. Components that provide reinforcement are embedded in the matrix, which is generally less stiff and serves as a binder to keep the reinforcing fibers in place. When an external load is applied, the continuous phase of matrix resin transfers load to reinforcing layers- ideally the external pressure is distributed evenly within the composite.

Fiber reinforced plastics (FRPs) are composites wherein fibers behave as the reinforcing component and polymeric resins as the matrix. Three commonly used reinforcement fibers are carbon, polyaramide, and glass fiber. Among these, carbon fiber has the highest properties of mechanical strength and stiffness. Polyaramide fiber have the lowest density, but glass fiber is the most economical. (See Table 2.1 for details on fiber density, tensile strength, and elastic modulus.)

Carbon fiber reinforced plastics (CFRP) are the focus of this research, because of their high values of strength-to-weight and specific stiffness. CFRPs are valuable materials for aerospace applications and construction. The fuselage of Airbus A310 are totally fabricated from carbon composites. CFRPs afford ~400 kg in weight savings when compared to aluminum (Al) alloy-based units that were previously used [2]. Weight

savings of 1 kg will in turn reduce fuel by 2900 L or more per year [2]. Moreover, CFRPs for use as airline fuselage also reduces the number of additional parts; 95 parts versus 2076 metal parts (excluding fasteners) for Al alloys. Thus, the CFRP based-fuselage is easier to manufacture. A CFRP-based C17 tail of 62 ft. was completed with 4300 fewer parts (including fasteners). The reported weight reduction was by 20% (260 kg less weight) and cost savings were 50% in comparison to the existing metal tail [2].

Table 2.1 The mechanical properties of common fibers in fiber reinforced plastics [1]

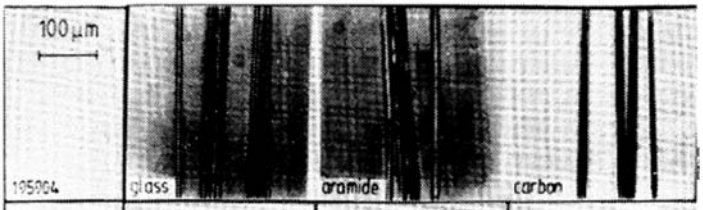

ρ [g/cm³]	2.5	1.45	1.8 (2.1)
σ_{Zug} [MPa]	2000-4000	3600 (3400)	3000-5000 (2000-3000)
E ∥ [GPa]	50-80	125 (180)	200-400 (400-700)

2.1.2 Carbon Fiber

2.1.2.1 The Structure of Carbon Fiber

The high strength and specific modulus of carbon fiber are attributed to its graphitic crystal structure, as shown in Figure 2.1. The basic unit cell geometry of the graphite crystal is the hexagonal ring, which has carbon atoms arranged in stacks of parallel sheets. The planar sheets of carbon are aligned along the fiber axis. Carbon atoms are held together by strong covalent bonds of 525 kJ/mol, while weak Van der Waals forces are less than 10 kJ/mol between atomic layer. As a result, carbon fiber's properties are highly anisotropic. The theoretical, in-plane Young's modulus is about 1,000 GPa, while the transverse

modulus is barely 35 GPa [2][3]. In fact, the crystalline structure of carbon fibers is not perfectly stacked in layers, but rather there is some disorder among carbon-sheets (as shown in Figure 2.1 which shows the turbostratic structure of commercial carbon fiber) [3]. The misalignment of graphitic plans decreases the axial strength of carbon fibers; however, this can improve mechanical properties affected by the transverse direction, such as compressive strength and shear strength. The misalignment of graphitic layers causes in-plane covalent bonding in the transverse direction.

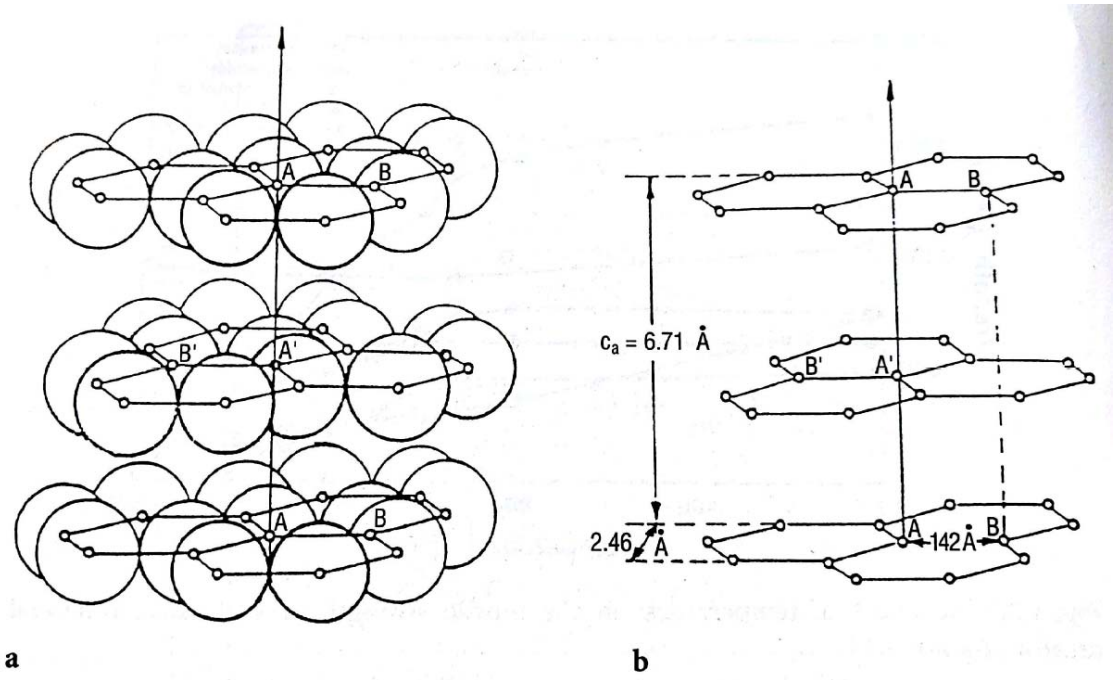

Figure 2.1 The anisotropic structure of graphite [3]

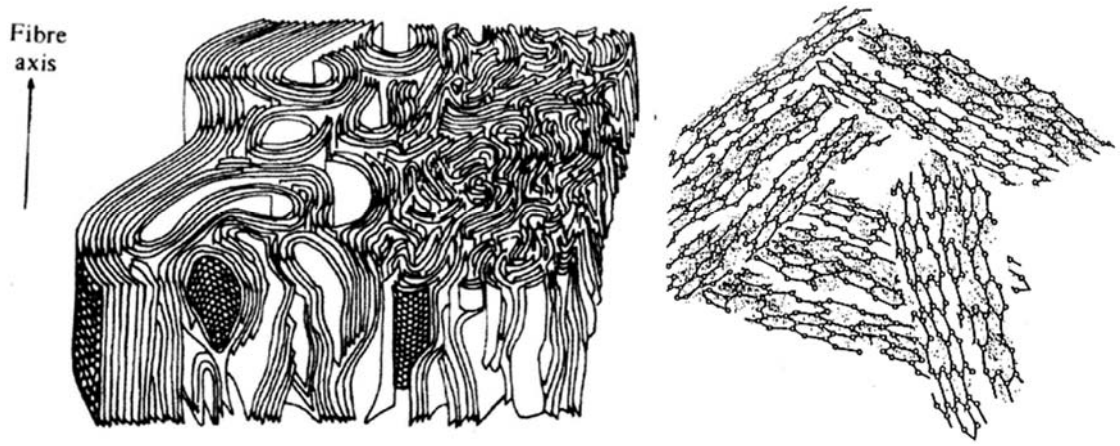

Figure 2.2 The turbostratic structure of graphite [3][4]. On the left is the schematic of carbon fiber structure, and right is one layer of bended graphite crystal structure

2.1.2.2 Precursor of Carbon Fiber

There are three commercially used precursors for carbon fiber production: polyacrylonitrile (PAN), pitch and Rayon (as shown in Figure 2.3). PAN carbonization is most suitable for the development of high strength carbon fibers. It is also the commercial standard [3]. The formation of graphitic carbon, having lattice spacings of 0.335 nm, for advanced applications is influenced by temperature and the removal of heteroatoms in inert environments. PAN dopes for fiber spinning are highly viscous. Polymer chains are stretched along the fiber axis to establish the preferred orientation of carbonized polymer. After high temperature oxidation (at 200-230 °C in air), adjacent nitrile groups cyclize in the form of laddered rings. Heteratoms are converted to carbon during carbonation at temperatures ranging from 1000-1500 °C under inert gas. The final heat treatment, under inert conditions at 2000-3000 °C, further enhances the Yong's modulus and tensile strength of carbon fibers. Ranges of Young's modulus fall into different categories: standard (230-240 GPa), intermediate (250-300 GPa) and high (350-500 GPa). Transverse modulus values are 3-10% of the Young's modulus [3][6].

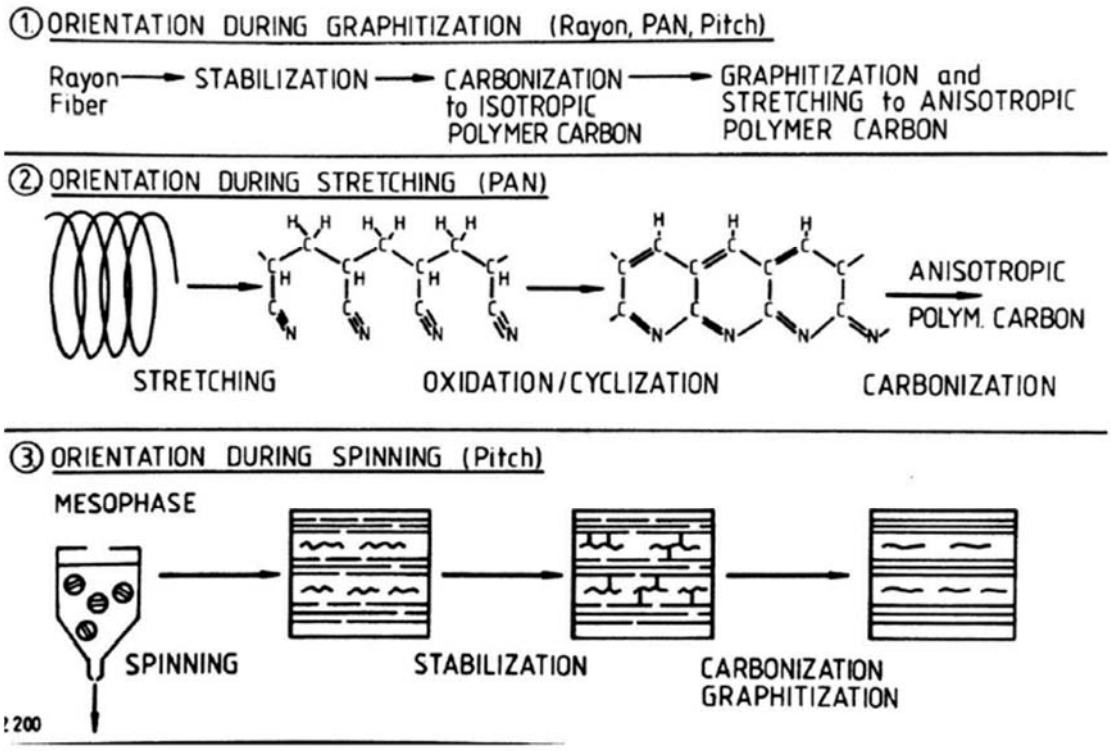

Figure 2.3 Three types of processes for fabrication of carbon fibers [1]

Pitch from petroleum and coal consists of aromatic carbons and heterocyclic compounds. When heated above 350 ° C, mixtures convert to mesophase pitch- a thermotropic liquid crystalline polymer- after condensation polymerization [6]. Molecular alignment is achieved after melt spinning mesophase pitch. Afterwards, melt-spun fibers are annealed in air below its softening temperature; this is called stabilization. Upon stabilization, molecular crosslinking occurs through the reaction of carbonyl and phenoxy groups [1]. Stabilization ensures the molecular structure of pitch-based fibers are infusible [1]. Before carbonization at up to 1,700 °C or graphitization at 3,000 °C (where high strength and modulus are achieved), stabilization or pre-carbonization, between 900-1,000 ° C, removes non-carbon elements [1].

Rayon fiber, regenerated from cellulose, is converted into carbon fiber by pyrolysis, as shown in Figure 2.4. Stabilization in air occurs at 200-350 °C, wherein glyosidic bonds release volatile carbon oxides and extensive weight loss occurs. Carbonization in an inert environment at 1000-2000 °C results in layers of carbon atoms. Graphitization occurs in an inert environment at ~3000 °C under tension to achieve the axial alignment of carbon structures. The aligning of graphitic structures is an extremely difficult process to perform and is also very expensive [9]. The Young's modulus is typically between 300-600 GPa [1].

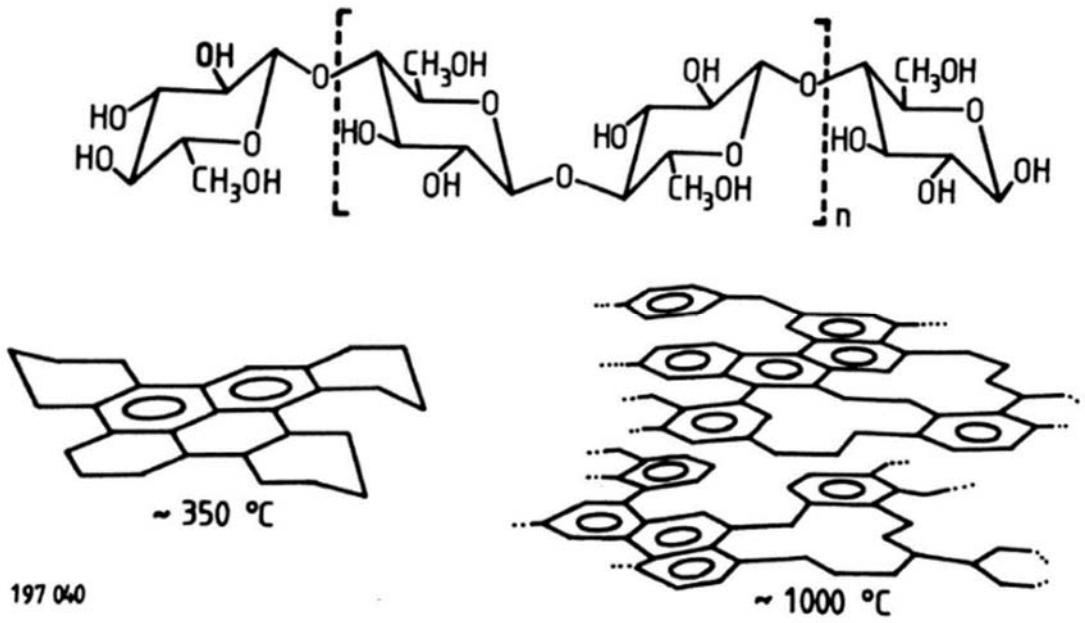

Figure 2.4 Thermal degradation of rayon to carbon

2.1.2.3 Carbon Fiber Architecture

Carbon fiber is manufactured in the form of thread-like bundles, i.e. tow. Standard tow sizes (number of filaments in one bundle) are 1k, 3k, 6k and 12k. For example, in 3k tow, there are 3,000 filaments. Tow size influences the strength and weight of CFRPs[10]. Tows are arranged in the CFRPs in different patterns or fabric geometries. Carbon fiber

geometries influence pore shape and distribution, fiber volume fraction in the CFRP, and fiber orientation. These inherent properties will affect the properties of CFRPs overall [3]. Geometries for continuous carbon fiber are divided into four categories: discrete, unidirectional, planar (two dimensional), and integrated (three dimensional) (see Figure 2.5). Geometries of discrete or chopped carbon fiber are fabricated into CFRPs by spray layup or the pulp molding of short fibers. It is hard to control the orientation and pore structure of these geometries. Fiber volume fraction is low, which in turn results in low CFRP strength.

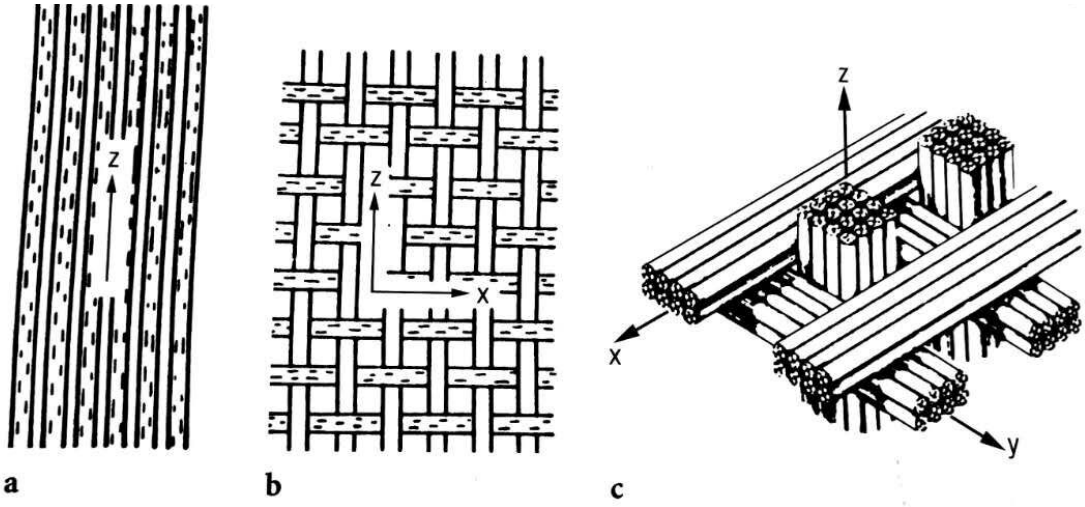

Figure 2.5 Three fiber architectures with continuous fibers. (a) unidirectional, (b) two-dimensional, (c)three-dimensional [11]

Unidirectional fiber within the CFRP renders the most efficient transfer of stress from matrix resin to fiber. The theoretical packing efficiency or fiber volume fraction is the highest among all geometries at 90.7% [6]. Nonetheless, the out-of-plane performance of CFRPs is particularly poor.

Planar geometries refer to two-dimensional woven fabrics; wherein orthogonal sets warp yarns (i.e. ends) and filling yarns (picks) are interlaced. Both warp and filling yarns are woven in patterns that are known to achieve certain performance requirements. Basic

geometries are the plain, satin and twill weaves (Figure 2.6.) Plain weave is the simplest weave. Warp and filling yarns cross over and under each other. The plain weave is the tightest weave, having good stability and low inter-yarn slippage. Satin weave is constructed when four or more warp yarns cross over a single filling yarn. Satin weaves have less inter-yarn lacing than the plain weave. In comparison to plain weave, the floating yarns of the satin contributes to denser fiber packing, higher mechanical strength, and modulus. The tightness of yarns within the twill weave is between that of the plain and satin weaves. The diagonal line seen across the fabric structure is a common distinction among twill weaves.

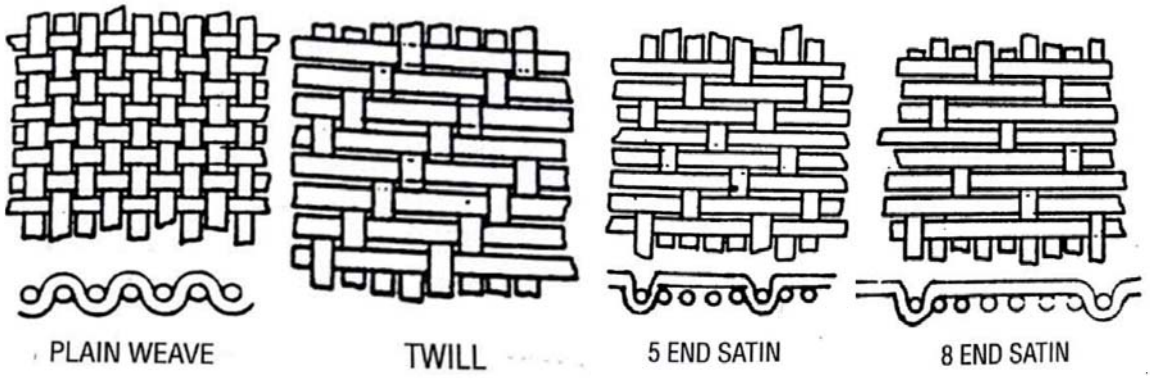

Figure 2.6 Basis weave pattern [3]

Three-dimensional (3D) geometries of carbon fibers have fibers aligned in all directions. The integration of yarn along the z-axis overcomes the performance limitations of planar fabrics, which are associated with low out-of-plane strength and poor interlaminar shear strength. Having yarn along the z-direction affects fabric thickness and fiber volume fraction (as shown in Figure 2.7). Three-dimensional carbon fabrics are typically fabricated by braiding, knitting, weaving, or needlepunching (most commonly used nonwoven in composite applications). Braiding is processed by intertwining (or the orthogonal interlacing of) three or more yarn systems. Knitting is designed by arranging yarns in a

repeating series of intermeshed loops. Nonwoven fabrics are reinforced by the needlepunch process that uses barbed needles to push fibers through the fiberweb's thickness. There are various techniques to form 3D woven structures. One of such structures is the 3-dimentional orthogonal woven structure, having three sets of yarns, x- y-, and z-yarns. The yarns in z-direction, known as binder yarns, provide structural integrity. Fiber volume fraction among these structures is dramatically varied from very low to very high levels. Figure 2.7 shows two examples of 3D orthogonal woven structures.

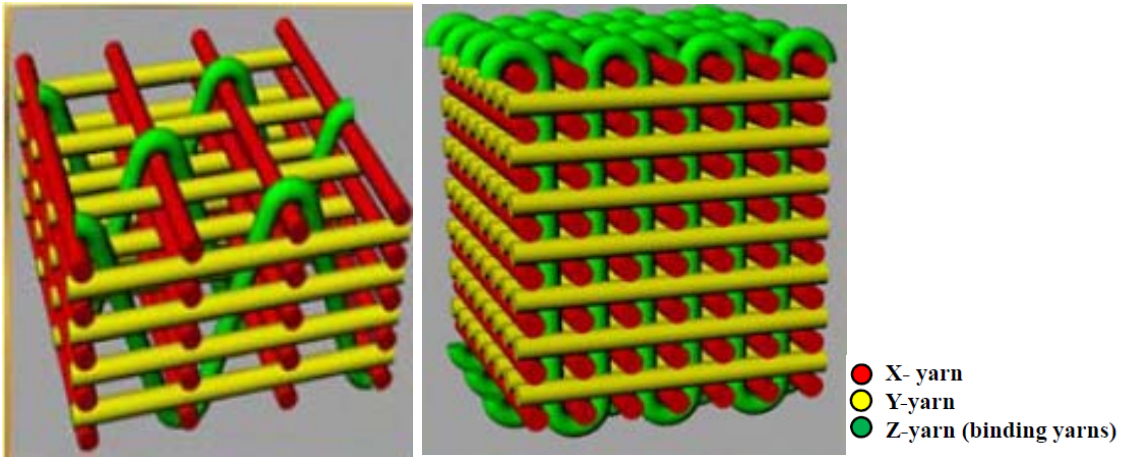

Figure 2.7 3D woven structure. Thin and open (left) & thick and tight (right). [1]

2.1.3 CFRP Matrix Resins

Matrix resins are either thermosetting or thermoplastic polymers. Thermosetting resins are cured at elevated temperatures to cause chemical reaction and intermolecular crosslinks. Thermoplastic resins having weaker intermolecular interactions holding the linear or branched polymers together [13] as shown in Figure 2.8. The strength and stiffness of thermoplastic resins are attributed to their chemistry and average molecular weight [6]. In comparison to thermosetting precursors, thermoplastic resins are more viscous and difficult to process. The molecular mobility of thermoplastic resins is affected by

[1] From course lecture "Advance Woven Fabric Design", by Dr. Abdel-Fattah Mohamed Seyam, 2016 Fall

temperature. Altering temperature can induce the solidification/melting of crystalline polymer or cause the entanglement/disentanglement of polymer chains. The highly-cross-linked structure restricts the molecular motion of cured thermosetting resins. Polyether ether ketone (PEEK) is the typical thermoplastic resins, having a semi-crystalline structure. Thermosetting resins have better creep resistance and maintain their shape over a range of temperatures. Also, thermosets have less strain to failure than thermoplastics, which results in their brittle nature.

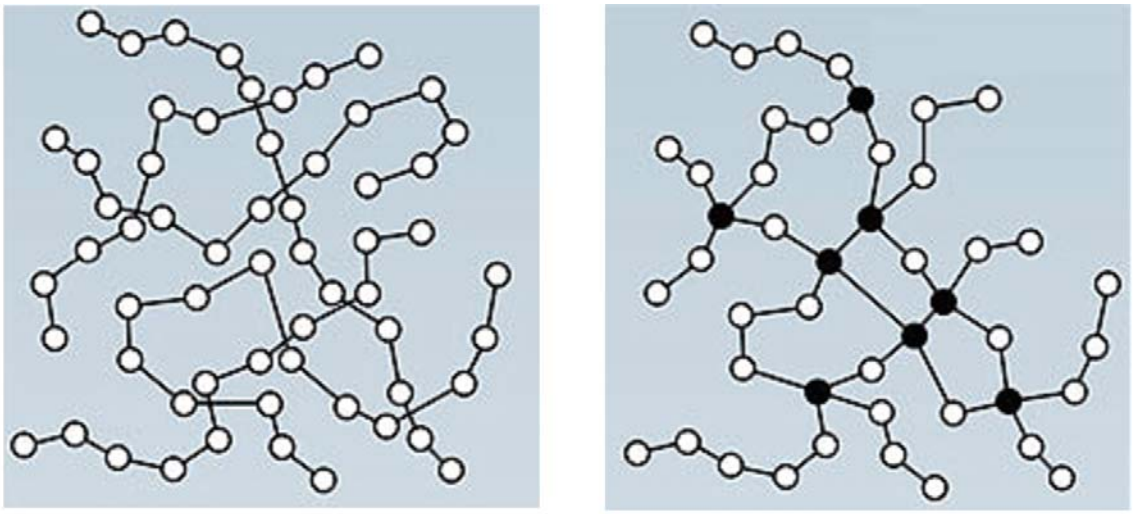

Figure 2.8 Thermoplastic and thermosetting matrix resins [12]

2.1.4 Delamination of CFRP

2.1.4.1 The Description of CFRP Delamination

The through-thickness strength of CFRPs is dominated by matrix resin, whose poor performance is due to its brittleness and poor interfacial adhesion with reinforcing fiber. Typical damage modes across CFRP cross-sections are illustrated in Figure 2.9. Delamination results from several failure modes. Cracking occurs as the brittle matrix resin and fragile interface between carbon fiber and matrix resin are unable to withstand impact. As the crack propagates, delamination inevitably results in failure- the point at which the

interlaminar shear stress exceeds interlaminar shear strength. Interlaminar shear stress is impacted by geometry and loading parameters, while interlaminar shear strength is decided by the material properties [5].

Sang-Jae Yoon et al. [15] applied acoustic emission (AE) technique to track delamination in the CFRPs. They summarized crack propagation into three stages (shown in Figure 2.10) where the shape of AE signal was burst with different amplitude and frequencies:

Stage 1: Crack initiation appeared after suffering from external load and cracks were stopped by the hardened resin;

Stage 2: Cracks propagated along the poor adhesive interface until at least 80% of the adhesion. The crack propagation was restrained and the strain energy accumulated at the crack tip;

Stage 3: The burst of accumulated strain energy exceeded the fracture toughness, and the crack jumped to another layer.

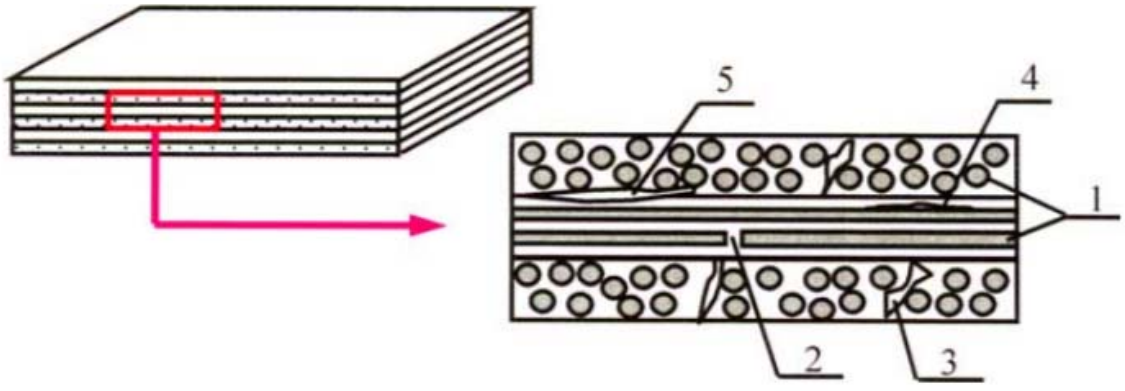

Figure 2.9 Scheme of damage mode in CFRP [14]:
(1) reinforcement fibers, (2) fiber breakage, (3) matrix crack, (4) fiber/matrix deboning, (5) delamination

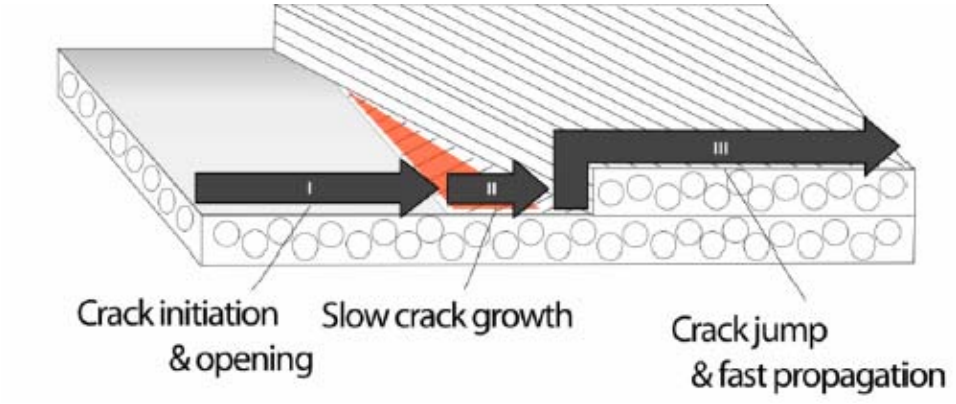

Figure 2.10 Illustration of the fracture behavior in response to tensile loading [15]

2.1.4.2 Previous Work to Decrease Delamination

The poor interfacial adhesion between carbon fiber and matrix resin limits the fracture toughness of the matrix. Poor fracture toughness is a primary contributor to delamination. Approaches to improve resistance to delamination include increasing the though-thickness strength, enhancing interfacial adhesion, and toughening matrix resin. Based on an understanding of failure modes, modifications to the matrix resin or fibers are used to improve the delamination resistance of CFRPs.

Carbon fiber surface treatment

Carbon fiber has an inert surface that prevents intimate contact with matrix resin. The use of surface treatments is a promising approach to enhancing the interfacial adhesion between carbon fiber and matrix resin. Surface treatments for carbon fiber include acid oxidation, plasma treatment, rare earth treatment, gamma radiation and etc. [17] These treatments modify the surface of carbon fibers in terms of their morphology and chemical composition. The formation of micro-pores is a morphological change along carbon fibers that results in more surface area. By increasing the surface area of carbon fibers, the overall fracture toughness of CFRPs is enhanced. Through micro-pores, matrix polymer

mechanically interlocks with carbon fiber. By introducing functional groups on the carbon surface, intermolecular bonding (through COOH, --C--OH and -C=O groups) can occur between the matrix resin and carbon fibers. The wettability of carbon fiber is improved obviously with both the increase of surface area and the change of surface chemistry.

3D woven fabrics

3D woven fabrics, as reinforcement, are integrated structures for CFRPs. Laminated carbon fabrics are stacked together in layers. 3D woven fabrics have fibers in the z-direction to strengthen composites along their through-thickness- thereby improving the delamination resistance. However, the laminated carbon fabrics can be tailored to meet the requirements of CFRP applications by placing each fabric at different orientations. Balancing the stacking sequence of fabrics for lamination is commonly used commercial practice. Compared to 3D wovens, which have one laminate orientation, laminated composites can better relieve local interlaminar stresses by counteracting loads from all directions [8].

Thermoplastic resins

Thermoplastic resins have been used to toughen CFRPs. For example, polyether ether ketone (PEEK) improved the overall ductility of the composite. But, PEEK's expensiveness and low processing ability restricts its use [18].

Toughening particles

Particles for toughening matrix resin exhibit plastic deformation upon external impact. Inter-particle bridging assists energy absorption by the CFRP [19][20]. During processing,

the dispersed particles increase the pre-cure viscosity of matrix resin. This makes the injection of resin into the CFRP mold more challenging.

Polymeric interlayer

Interlayers in the form of films or fibrous veils, containing microfibers or nanofibers, are used to improve the fracture toughness of CFRPs. Ductile, low glass temperature films bind with matrix resin to absorb energy upon deformation [21][22]. Nonporous films restrict resin flow during CFRP molding. Fibrous veils are the better choice for strengthening CFRPs than films.

Modes of energy absorption by using veils within CFRPs include fiber bridging, fiber pull-out, fiber deformation, and phase separation. Their porosity aids their wettability. Although nanofibers compose a low percentage of the composite (lower than 1% weight percentage of composites), these can significantly increase the fracture toughness of matrix resin- but not always. Kuwata et al. observed different ranges of CFRP toughening with interleaves: high, moderate and even negative effects [16]. The carbon fabric weave and matrix resin (epoxies are most commonly use) influence interleave performance. Toughening by means of interleaves were based on good interfacial bonding between the interleave and matrix. Fiber ductility, size distribution, and porosity affected interleave performance in the composite [16].

2.1.4.3 Nano-interleaves to Toughen Matrix Resin

Nanofibrous interleaves are fabricated directly onto carbon fabric or placed onto carbon fabric once in the form of sheets. Afterwards, these hybrid materials are molded into composites. Fracture toughness is often measured according to mode I and II fracture

mechanics. The double-cantilever beam (DCB) for mode I and end-notched flexure (ENF) testing for mode II. Fracture toughness is reported as Mode I and Mode II critical strain release rate (G_{IC} and G_{IIC} in J/m^2, respectively). Polycaprolactone (PCL) [8], polyacrylonitrile (PAN) [9][15], polyamide (PA) [10], polyamide 6,6 (PA 6,6) [11][14], polyvinylidene fluoride (PVDF) [12], polysulfone (PSF) [13], PEEK [26], polycarbonate (PC) [34] have been studied as nanofibrous interleaves for their effects on the fracture toughness of matrix resin.

Fiber bridging

Fiber bridging across cracks within the matrix resin results from the pulling of interleaved nanofibers, their deformation, and subsequent fiber breakage. Shafi et al. [15] incorporated carbon nanofibers, in the form of bucky paper, as a mid-plane layer within the CFRP. Mode II interlaminar fracture toughness of the composite changed by 105% upon adding the carbon nanofiber interleave. SEM images (in Figure 2.11 taken along the edge ENF test specimen) show carbon nanofibers are embedded throughout the matrix. Carbon nanofibers show bridging across broken matrix polymer or they were pulled out of the matrix, as shown in Figure 2.11B (c, d). Zig-zag crack pattern was observed throughout the sample containing interleaves, which is different from the relatively straight crack path that is among neat the CFRP. Thus, the energy consumed during crack propagation improved the fracture toughness of CFRPs containing interleaves. Based on Figure 2.12 of an ENF test specimen, it was evident that matrix resin nearest to the carbon nanofibers were rougher than resin shown in CFRPs lacking the interleave. The highly-deformed matrix resin indicated greater resistance to delamination.

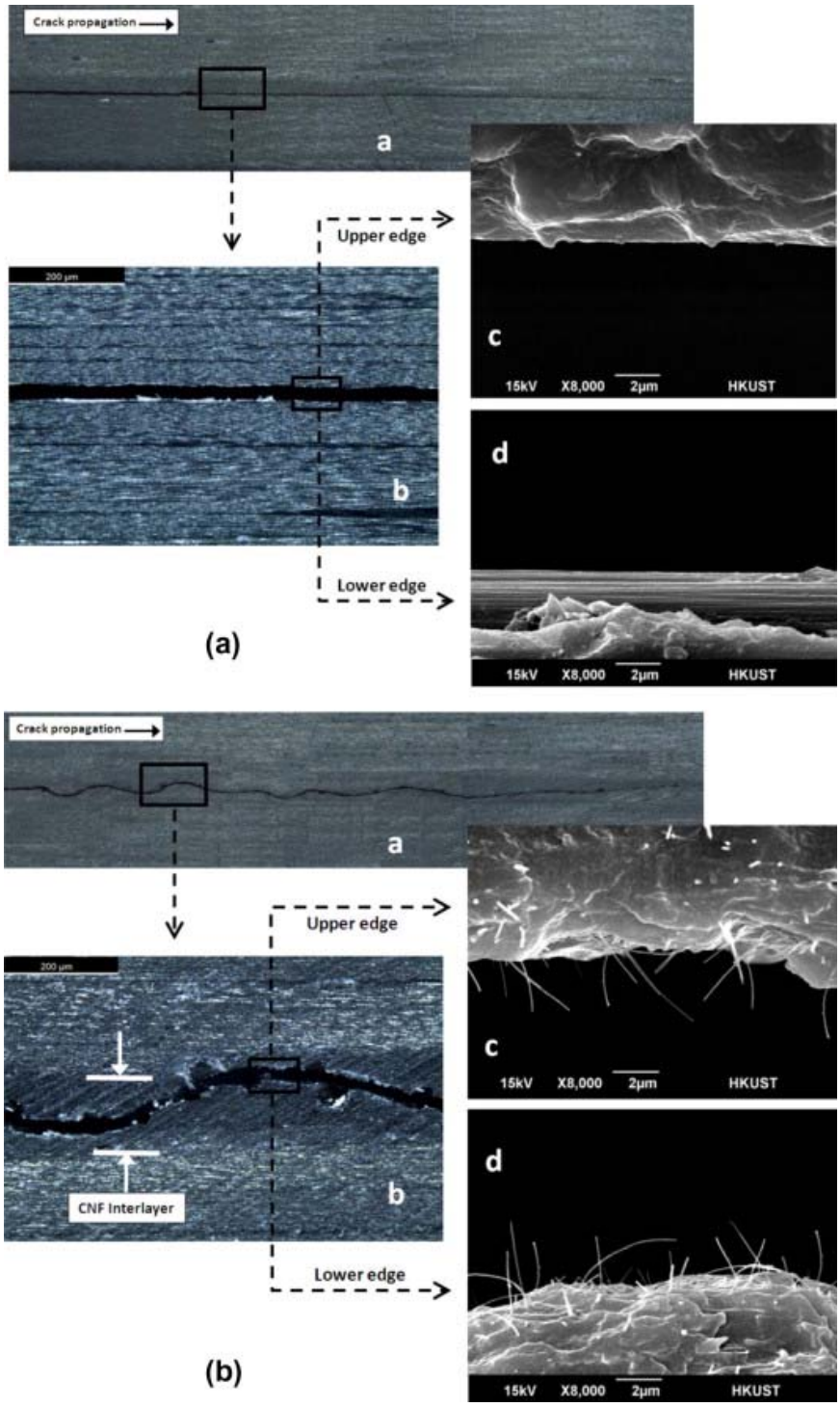

Figure 2.11 SEM images taken from the ENF test sample edges: (A) without interleaf, and (B) with an interleaf, where (a) general rack propagation pattern, (b) enlarged view of (a) and (c) SEM images of the upper and (d) lower edges.

[15]

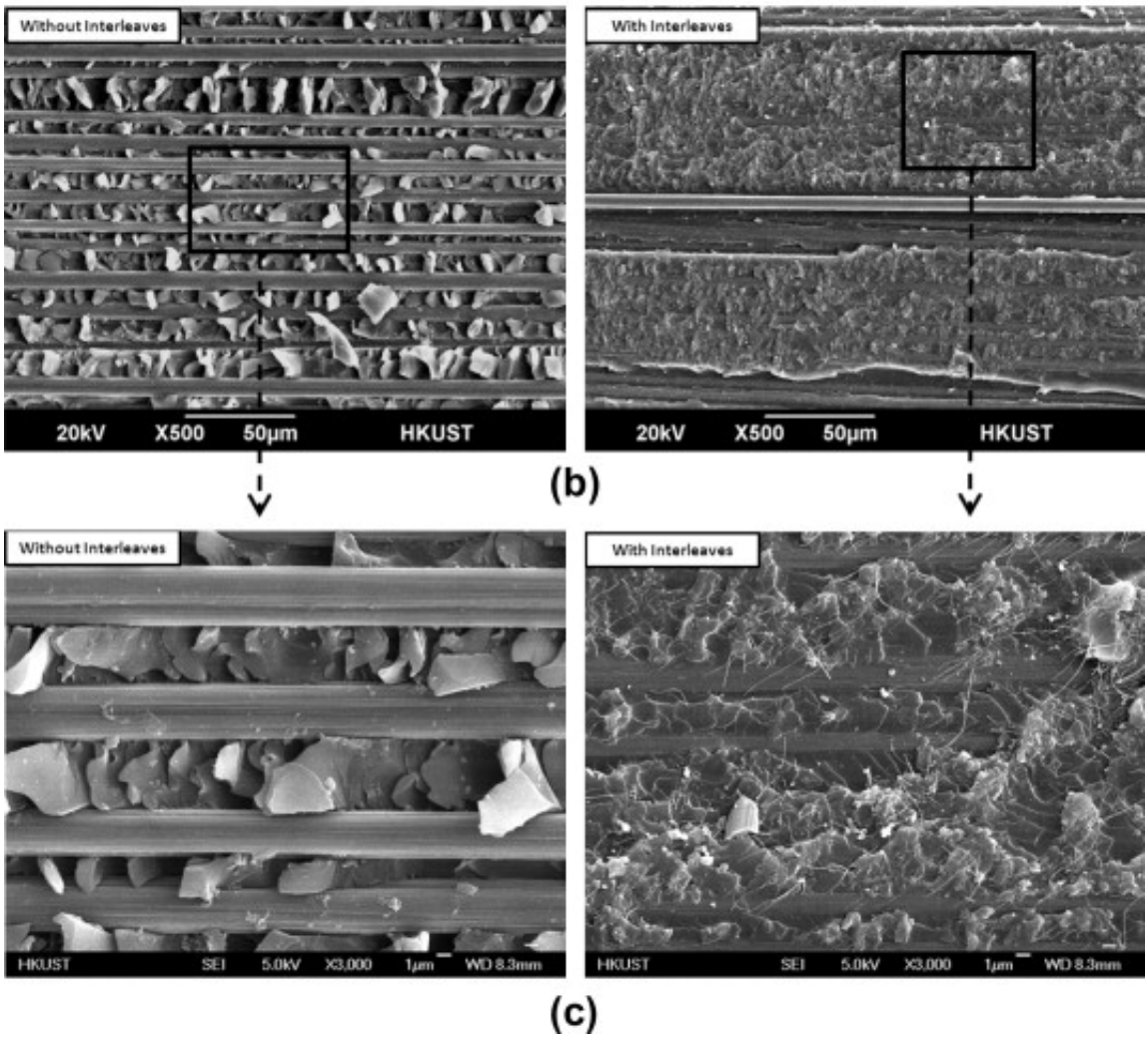

Figure 2.12 SEM images of the fracture surface of ENF test specimen with and without interleaves taken at low and high magnifications. [15]

SEM images of the CFRP fracture surface after DCB testing are shown in Figure 2.13; brittle fracture is contrasted with ductile fracture on the right [24]. Masahiro et al. [24] investigated the use of carbon nanofiber as interlayers that toughen CFRPs. An interlayer, having a basis weight of 20 g/m^2, showed greater toughening than layers of 10 and 30 g/m^2. G_{IC} increased by 50%, and G_{IIC} improved by 2-3X the CFRP without interleaves. Hardik et al. [25] also studied the effect of basis weight on interleave layer-induced toughening. 2-layered, 4-layered and 8-layered carbon nanotube (CNT) sheets weighed 0.354 g/m^2, 0.708 g/m^2 and 1.41 g/m^2. Each layer was laid in the middle of woven

glass fiber plies to improve the interlaminar fracture toughness of the composite. Only the 2-layered CNT embedded composite demonstrated an increase in G_{IC}. The fracture surface of composites containing 4-layered and 8-layered CNT sheets showed the presence of excessive nanotubes which allowed the crack to travel easily through the middle plane.

Lode et al. [27] applied electrospun PA 6,6 nanofibers as interleave in the CFRP. Mode I and Mode II fracture toughness improved. In the interleave rich zone, PA nanofibers visibly exhibited plastic failure by necking. Nanofibrous bridging occurred in the deformed regions of matrix polymer until the matrix eventually broke.

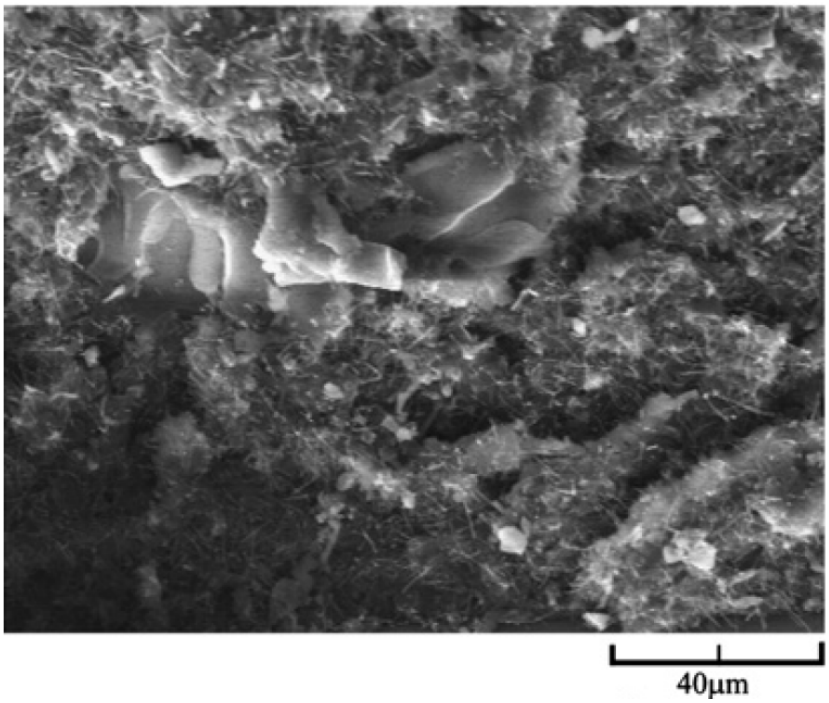

Figure 2.13 SEM images of the fracture surface of DCB test specimen with and without interleaves. [24]

Phase separation

Composites are thermally cured during fabrication. Curing temperature can affect the state of interleaves, because theses solid nanofibers can soften into liquid when heated above their glass transition temperature or melting temperature. Heating can introduce another toughening mechanism- known as phase separation. Jin et al. [9] used PCL, PVDF and PAN nanofibers as interleaves in the CFRP. The melting temperature for PCL and PVDF were 60℃ and 165℃, respectively, but PAN degrades without melting. Composites were cured at 125℃ for 1.5 h and then 175℃ for 2 h. Based on G_{IC} results, PCL barely toughened CFRPs. PVDF and PAN nanofibers had negligible or a negative performance effect. Figure 2.15 shows only PEEK and PCL were miscible in the epoxy matrix. PVDF and PAN were immiscible with epoxy. Epoxy polymerization upon curing induced phase separation, as shown in Figure 2.14b, c, and d. The thermoplastic-rich phase enhanced interlaminar fracture toughness by resisting crack growth and propagation [9]. Gang et al. [13] reported polymerization-induced phase separation after epoxy curing, as well. Spheres were uniformly dispersed between the interleaves of the CFRPs. Jin et al. [26] varied the diameter of PEEK nanofibers placed in the CFRP at 450, 750, and 950 nm. The finer fibers reduced the distance between PEEK rich phases therefore stabilizing the crack propagation. Nan et al. [69] sandwiched CNT/PSF interleaves within CFRPs. PSF was dissolved by epoxy during curing. Phase separation in the form of microspheres in the epoxy were observed, while CNTs dispersed in the epoxy served to restrict crack propagation throughout matrix resin.

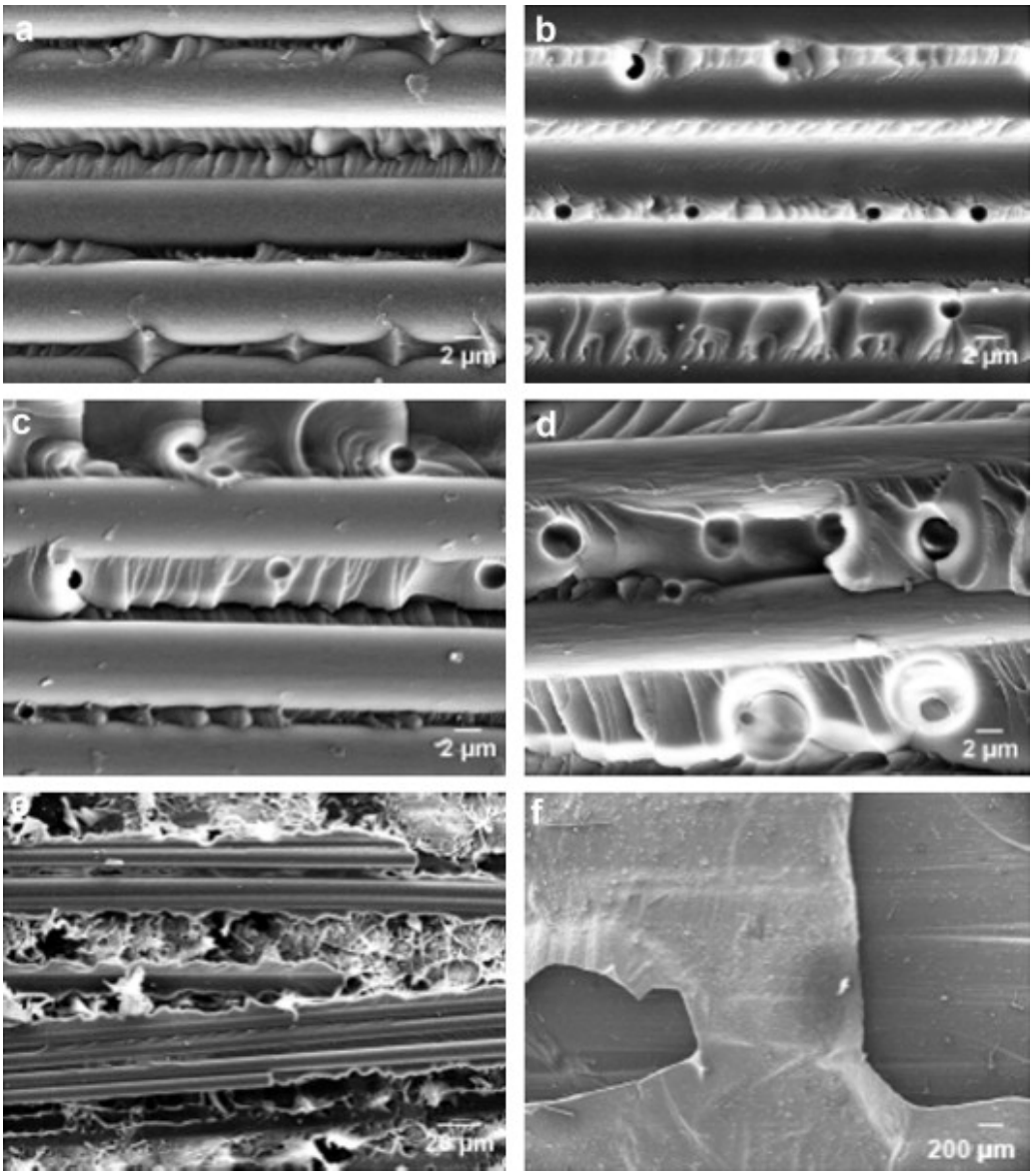

Figure 2.14 SEM images of fracture surface under DCB test. (a) control sample, (b-d) samples toughened by PCL nanofibers with concentration from 12 wt %, 15 wt %, 20 wt %, (e, f) samples toughened by PVDF and PAN [9]

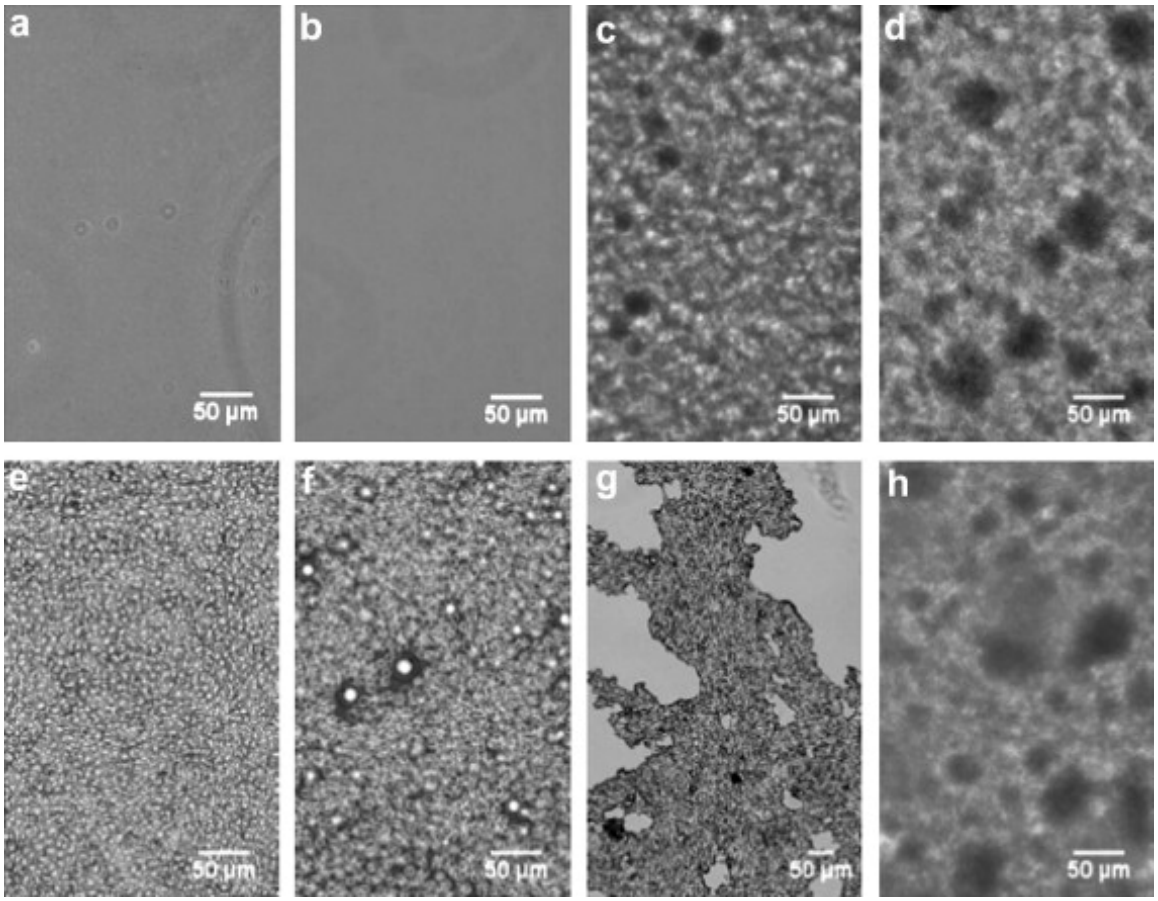

Figure 2.15 Optical micrograph of thermoplastic/epoxy blends before (top) and after curing (bottom). (a, e) PEEK, (b, f) PCL, (c, g) PVDF, (d, h) PAN [9]

2.1.5 Summaries and Conclusions

The unique graphitic structure of carbon fiber attributes to its superior strength and stiffness. These light-weight materials, having excellent mechanical strength, make CFRPs promising structural materials. Delamination is the main fracture mode of CFRPs. It results from poor interfacial adhesion between carbon fibers and the brittle matrix resin. Many means have been put forth to improve the delamination resistance of CFRPs. The addition of nanofibrous interleaves is a promising process for improving fracture toughness without significantly increasing the composite's weight or complicating CFRP manufacturing.

2.2 Electrospun Nanofibers

2.2.1 Introduction to Electrospinning

The fabrication of nanofibers is an extremely important topic. Nanofibers have high values of specific surface area due to their very fine fiber diameter [35][37]. Their high values of specific surface area and porosity enable chemical reaction, which increases their capture efficiency as filter media. There are many methods to fabricate nanofibers; such as electrospinning, self-assembly, template synthesis, and thermally-induced phase separation [35], melt blowing, and centrifugal spinning. Electrospinning is the most popular technique. There are a variety of electrospinning set-ups: Each ranging in terms of operational cost and simplicity of use. Further, various polymers are used to electrospin continuous nanofiber. Control of fiber diameter and morphology are possible to some degree.

Electrospinning technologies are not limited to laboratory use. Commercial applications for electrospun nanofibers (such as filters, catalysts, and reinforcement layers) have resulted in their large-scale production. Moreover, electrospun fibers have potential use in biological applications; such as tissue engineering, wound healing, drug transport and release, tumor and inhalation therapies [35].

2.2.2 Electrospinning Process

As shown in Figure 2.16, a laboratory electrospinning setup may comprise of a capillary tube (spinneret), high voltage supply, and collector [35]. Molten polymer or dope are continuously pumped through the charged capillary tube. At the tip of the capillary, the hemispherical drop becomes a charged Taylor cone at high voltage (10-60 kV). The threshold angle of the Taylor cone is 33.5° [35][41]. When the electrostatic force on the polymer droplet is large enough to overcome its surface tension, elongated jets stretch

towards the collecting screen. Collectors are either placed vertical or horizontal to the capillary tip. The jet path spirals outward as it approaches the collector; the fiber diameter simultaneously decreases. [35][37][38][39].

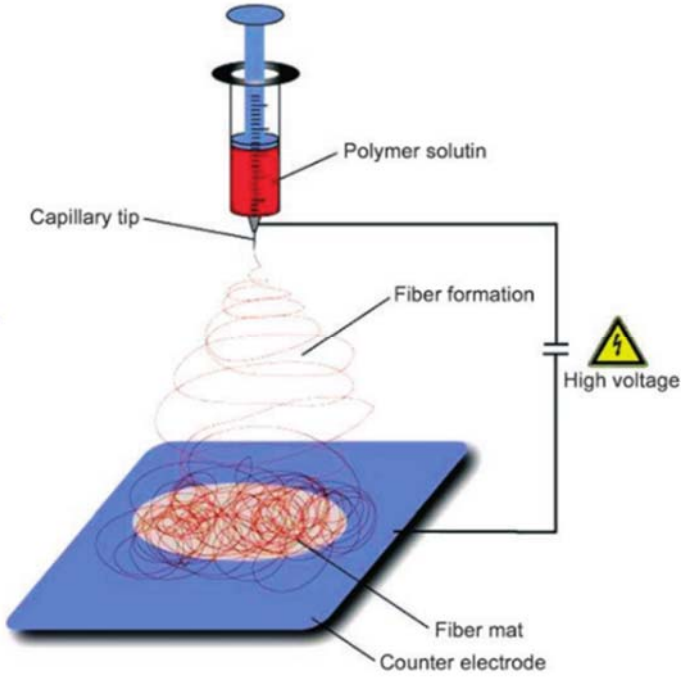

Figure 2.16 Electrospinning setup with horizontal collector in laboratory scale [37]

Fiber formation along the jet trajectory can be divided into three stages: jet initiation where the straight jet is formed, jet thinning describes its elongation towards the collector, and jet solidification into dry fiber [35]. Jet thinning influences fiber dimensions, its morphology, and physical properties. As the charged jet is stretched, it can split into multiple sub-jets that spray outward due to charge repulsion. Hohman et al. [40] described three categories of jet instability under an electric field. Axisymmetric Rayleigh instability is the dominant effect. Both axisymmetric and non-axisymmetric “whipping” instabilities contribute to fiber spinning at the nanoscale. Jet solidification is observed during the whole process. Solvent evaporation dictates nanofiber morphology in terms of beading and pore size.

2.2.3 Characterization of Nanoweb Structure

Nanoweb structure is described in terms of average fiber diameter and size distribution, fiber orientation, basis weight, pore size and the longitudinal shape of nanofibers [35]. Nanoscale fibers having a narrow fiber diameter distribution is important for filters. Variability in fiber size can adversely affect the pore size distribution towards larger pores, which results overall in low filtration efficiency. Pores affect impact air/fluid permeability, filtration efficiency and the mechanical properties of fabric [46]. Fiber orientation distribution influences the physical properties of nanofibrous webs (such as their strength, stiffness and fluid transportation). The orientation distribution function, Equation 2.1., characterizes fiber orientation in reference to machine or cross machine direction, where ϕ represents the fiber orientation. Basis weight (or areal density) is defined as the mass per unit area. This parameter affects liquid retention and the stiffness of nanofibrous webs [45]. Web structure is customized towards the application. Electrospinning parameters are tuned to achieve those properties.

$$Ht = 2\langle \cos^2\phi \rangle - 1$$

Where

$$\langle \cos^2\phi \rangle = \int_{-\frac{\Pi}{2}}^{\frac{\Pi}{2}} f_t(\phi)\cos^2\Phi d_\Phi$$

1 indicates a perfect alignment parallel to the reference direction

0 indicated randomness

-1 indicates a perfect perpendicular alignment to that direction

Equation 2.1 Overall Anisotropy Parameter function [42][43]

2.2.4 Electrospinning Parameters

Although electrospinning setups range in simplicity, controlling fiber properties is not so easy. Nanofiber morphology is dependent upon interrelated, electrospinning parameters. Electrospinning parameters divide into three types: solution parameters, process parameters, and ambient parameters. Solution parameters include viscosity, polymer concentration, conductivity and surface tension; process parameters include feed rate, electric field strength, geometry of the electrodes, hydrostatic pressure in the dispensing capillary, voltage potential at the tip, tip-to-collector distance (TCD), and the grounded collector; and ambient parameters are describe by the surrounding humidity and temperature [35][37][38][39][40].

Experimental testing is key to understanding processing and property relationships. Thompson et al. [42] proposed the systematic evaluation of electrospinning parameters on web morphology. Thirteen parameters were classified in terms of their influence on web structure. Factors affecting fiber diameter were classified as strong, moderate, or minor. The most significant parameters were volumetric charge density, distance from nozzle to collector, initial radius, relaxation time, and viscosity. Select parameters were tested against their effects on web structure (fiber diameter, diameter distribution, and fiber orientation) in this study.

2.2.5 The Effect of Electrospinning Parameters on Fiber Diameter

Solution-electrospinning produces fibers on the order of a few nanometers [35][37], while the melt-electrospinning of polymers like low-melting temperature PCL [47] were less than 400 nm. The high viscosity of molten polymer leads to larger diameter fibers.

Solution-electrospinning is more promising in its ability to produce nanofibers. Therefore, the following discussions are based on fibers electrospun from solution.

Viscosity

Dilute polymer solutions behave as a Newtonian fluid. The concentration of polymer in solution is proportional to its solution viscosity. In general, increases in polymer viscosity and concentration causes fiber diameter to also increase [48]. But if polymer viscosity is too low, surface tension- being far greater than the molecular cohesion of polymer chains- will cause the solution to electrospray in the form of droplets rather than electrospin as continuous fiber. On the contrary, polymer solutions having too high polymer concentration, will fail to electrospin as fiber, because intermolecular cohesion is too high. Deizel et al. [48] used PEO/water solutions whose concentration was between 4-10 wt % and viscosity ranged from 1-20 poise. Fibers did not form under the applied electric field when fluid viscosity was below 1 poise or over 20 poise. Vince et al. [49] reported electrospun polycaprolactone (PCL) fibers, where fiber diameter increased with solution concentration up to 20% polymer. Fiber formation was controlled by polymer chain cohesion.

Surface tension

Sergey et al [42] qualitatively analyzed the influence of several electrospinning parameters on fiber diameter. Surface tension was a primary factor. Thompson et al. [50] opposed reports that there was no noticeable relationship between surface tension and fiber diameters. The experimental data in support of this conclusion came from a combination of reported literature and their own model. In the image, the abscissa represented the

surface tension and the ordinate indicated the diameter. Related literature had shown surface tension mainly affected beading among nanofibers [37][39][49]. The relationship between surface tension and fiber diameter was unclear.

Conductivity

In an experiment conducted by Tan et al. [51], N,N-dimethylformamide (DMF) was used to enhance the conductivity of poly(L-lactid acid) (PLLA)/dichloromethane (DCM) solution. The decrease in electrospun fiber diameters was observed as the proportion of DMF in the solution increased. As conductivity of the polymer jet increased, polymer was loaded with more electric charge. Repulsion of like charge on the nanofiber surface led to finer fibers- resulting from greater jet elongation [37][52].

Flow rate

Shamim et al studied the effect of changing flow rate on fiber diameter. [53]. At optimum flow, the Taylor cone forms and fibers stretch towards the collector. Images of the Taylor cone shows fiber ejected from a droplet- either a single fiber or several fibers will splay towards the collector. At low supply, the applied charge is incapable of stretching the polymer jet. Fiber diameter increases as flow rate is optimized, concluded Thompson et al. [42]. There is an appropriate balance between flow rate and applied charge to obtain fibers.

Applied voltage

The fiber diameter decreases as applied voltage increases. Higher applied voltage results in more electrostatic charge on the droplet surface [53]. In consequence to higher flow rates [53] and excessive charge on the droplet surface [15], the fluid jet can split into

multiple sub-jets. Vince et al. [49] applied voltages of 10, 15, and 20 kV to polymer solutions. In doing so, they observed evidence that fiber diameter decreased significantly as voltage increased- when other variables were held constant.

Tip-to-collector distance

Teeradech et al. [55] and Weiwei et al. [56] reported longer tip-to-collector distances led to thinner fiber diameters. Thompson et al. [42] predicted that jet instabilities was the major cause of fiber thinning during electrospinning. The range for tip-to-collector distance depended on whether or not the desired fineness of fibers was obtained. If fibers solidify prior to reaching the collector, the relationship between nanofiber size and tip-to-collector distance becomes less predictable.

Temperature and humidity

With the increase of the ambient temperature, solvent evaporation increases during electrospinning. Increasing the temperature of the polymer solution also reduces the viscosity. These responses to temperature have different effects on fiber diameter. A lower solution evaporation rate means the electrospun polymer has enough time elongate under the applied electric field before solidification. Similarly, by reducing the viscosity of polymer solution, polymer chains can move more freely in solution. The effect of humidity on the fiber diameter is impacted by polymer chemistry [68]. S. De Vereze et al. [68] electrospun cellulose acetate (CA) and poly(vinylpyrrolidone) (PVP) under different conditions of relative humidity and temperature. Results indicated the raising of temperature increased PVP fiber diameter. CA diameter also dropped at higher temperature. With increases in humidity, PVP fibers were larger in diameter than CA fibers. Solvents

for PVP and CA were ethanol and a mixture of acetone/N,N-dimethylacetamide (DMAc). These solvent systems had different chemical affinities for water, where evaporated moisture was absorbed by PVP solution at a slower evaporation rate. However, moisture under ambient conditions accelerated the precipitation of CA- prohibiting jet stretching towards smaller fibers.

The influence of key electrospinning parameters on fiber diameter were described as though having separate effects, but an understanding of complimentary and even opposing affects from multiple parameters is more realistic. Some parameters are unpredictable, it is unmeaningful to discuss them individually. Lee et al. [39] utilized methyl chloride (MC) to dissolve poly(1-caprolactone) (PCL), DMF was added to modify solution properties. As the proportion of DMF to MC increased, the surface tension and viscosity of the solution decreased. But higher values of solution conductivity were observed. Adding DMF produced thinner fibers. All electrospinning parameters affected fiber morphology. Being acquainted with the individual impact of electrospinning parameters, can then give a greater appreciation for more complex relationships between parameters.

2.2.6 Fiber Diameter Distribution of Electrospun Fibers

Fiber diameter distribution is an efficient tool to characterize the size uniformity. Beads are the main defect at low concentration; their presence reduces uniformity. This will be discussed in more detail later. Andreas et al. [37] stated some electrospun fibers were not round but rather flat ribbons. As the polymer concentration increased, electrospun fibers became more cylindrical; fiber diameter distributions were narrower, as well.

Lee et al [39] discovered that when MC was the only solvent used for PCL without the addition of DMF, electrospun fibers were relatively larger in diameter and had a narrower diameter distribution. Spraying and splitting were not observed during electrospinning. Demir et al. [54] described the morphology of electrospun fibers from polyurethane. More than one jet ejected from the charged dope. As a result, the distribution of fiber diameters was wide. Shamim et al. [53] investigated the influence of flow rate on fiber diameter distribution. Their results showed the narrowest diameter distribution of electrospun fiber occurred under the flow rate of 0.5 mL/hr.

Literature describing the effects of ambient temperature on electrospinning is limited. Demir et al. [54] compared the morphologies of polyurethane fibers that were electrospun at room temperature to those spun at 70 °C. Polyurethane fibers spun at the higher temperature were significantly more uniform in size.

2.2.7 Orientation of Electrospun Fibers

Fiber orientation is defined as the angle between the axial machine direction (MD) of fiber to the cross-machine direction (CD) of the formed web [39]. Usually, conductive plates and rotating drums serve as collectors, see Figure 2.17. The web formed on a conductive plate will have random orientation, while the rotating drum is used to align the fibers within the web [35][37][39][58][59][60]. Recently, continuous uniaxial fibers are targeted to expand applications. Several collector technologies have been attempted for fiber alignment [35][58]. Jet bending, which happens during fiber formation, makes it difficult to align fibers uniaxially [35]. The linear velocity of the drum is important for controlling web alignment. In general, more alignment in the MD direction occurs at higher velocity. The effective draw of fibers at the drum surface is important for alignment

[35][59][60]. While if the take-up surface velocity is far higher than the speed of fibers formation, consequently, fibers are broken up [35]. Other novel approaches to align nanofibers include using a drum frame of steel wires as the collector, modulation of the electric field, placing the fiber collector between two narrowly spaced electrodes; adding magnetic materials (such as Fe_3O_4) to the dope and then placing magnets along the edge of collector. [35][66][67]

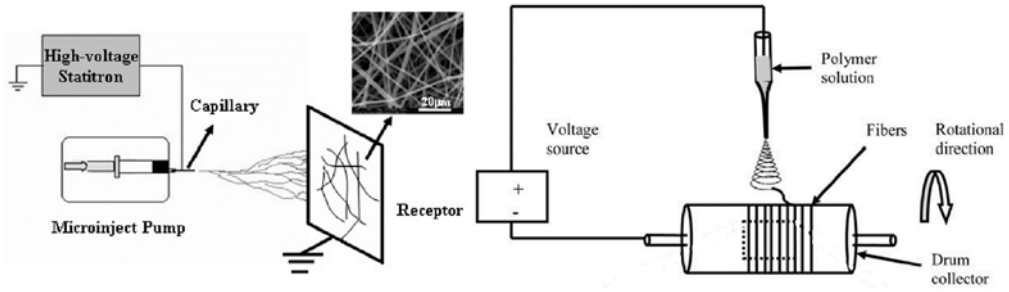

Figure 2.17 Collectors of the conductive plate (left) and rotating drum (right) [57][58]

2.2.8 Morphology of Electrospun Fibers

Beads are common but undesired by-products of electrospinning. They decrease the specific area of nanofibers [54]. Hence, the surface tension and viscosity of dopes are manipulated to eliminate beads. Polymer concentration influences solution viscosity. Thus, polymer concentration is controlled to allow for the electrospinning of beads-free nanofibers [62][63][64] . Silke et al. [63] dissolved polystyrene (PS) in tetrahydrofuran (THF). The appearance of beads decreased as PS concentration increased, see Figure 2.18. As polymer concentration or solution viscosity increases greater cohesion among polymer chains exist to exceed the surface tension of the solvent. Experiments have also proved that lowering surface tension produces electrospun fibers without beads [35][61]. By increasing dope conductivity, excess charge accumulates along the dope when voltage is applied. In

turn, the jet stretches to preclude bead formation [60]. Conductive additives is added to the dope to increase conductivity and charge density. These additives include salts and surfactants [35][61][62][65]. Tong's et al. [65] investigated the addition of tetrabutylammonium chloride (TBAC) to PS. This surfactant enhanced solution conductivity without affecting its viscosity. Beading was prevented when less than was 10^{-6} mol $^{-1}$ surfactant was added.

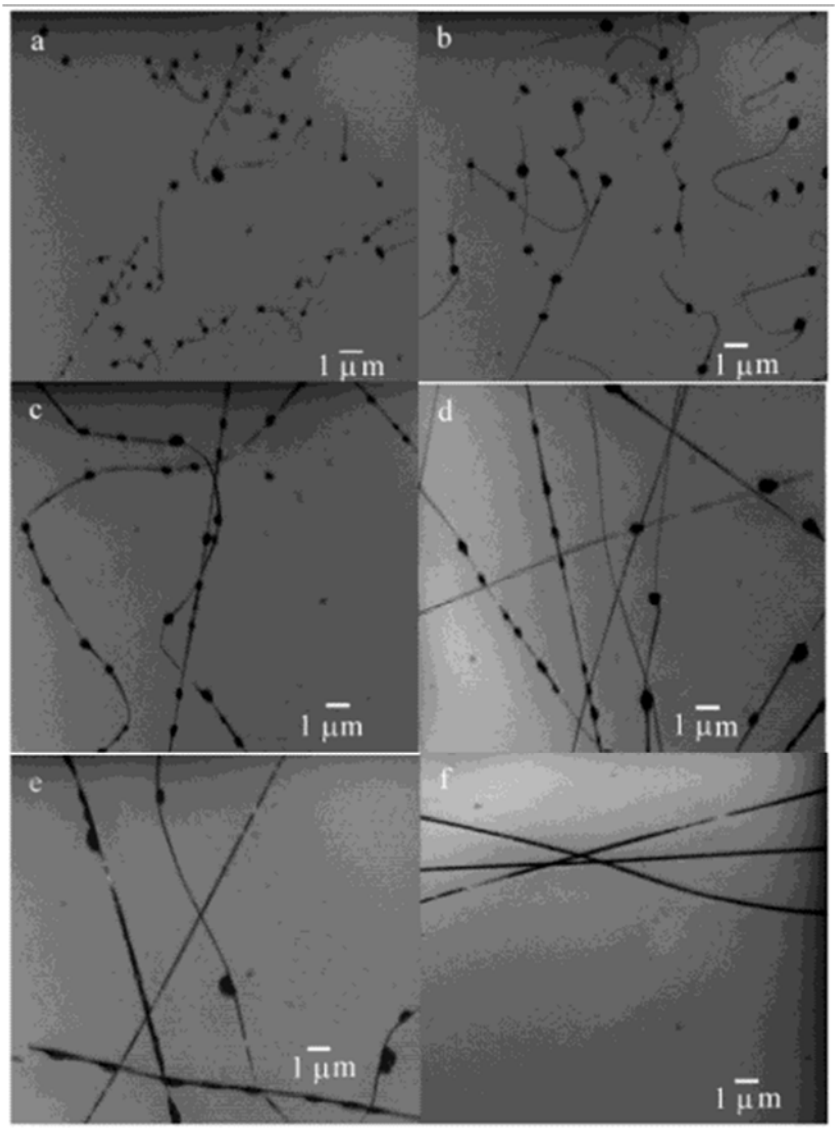

Figure 2.18 Optical microscope images with the increase of PS concentration.

(a) 18 wt %; (b) 20 wt %; (c) 25 wt %; (d) 28 wt %; (e) 30 wt %; (f) 35 wt %.

2.2.9 Summaries and Conclusions

The relationships between electrospinning (solution, processing, and ambient) parameters and web structure were discussed in detail. In summary, fiber diameter will decrease with decreases in viscosity and flow rate. As the applied voltage, solution conductivity, and tip-to-collector distance increase; the fiber diameter will decrease. Narrow fiber diameter distribution is produced at optimum surface tension and solution viscosity. Polymer concentration, conductivity and dielectric constant also influenced the diameter distribution.

Fiber orientation distribution represents fiber alignment along the MD direction, as the speed of take-up collectors are increased. Beads along nanofibers are eliminated as polymer concentration increases along with solution conductivity. Further, surface tension must decrease to remove beads from along the nanofibers. In this study, several parameters were used to optimize nanofiber morphology.

References

[1] Figueiredo, José Lùis, et al., eds. *Carbon fibers filaments and composites*. Vol. 177. Springer Science & Business Media, 1990.

[2] Soutis, C. "Carbon fiber reinforced plastics in aircraft construction." *Materials Science and Engineering: A* 412.1 (2005): 171-176.

[3] Fitzer, Erich, and Lalit M. Manocha. *Carbon reinforcements and carbon/carbon composites*. Springer Science & Business Media, 2012.

[4] Bennett, S. C., and D. J. Johnson. "Structural heterogeneity in carbon fibers." *Proceedings of the Fifth London International Carbon and Graphite Conference*. 1978.

[5] Nasuha, N., A. I. Azmi, and C. L. Tan. "A review on mode-I interlaminar fracture toughness of fibre reinforced composites." *Journal of Physics: Conference Series*. Vol. 908. No. 1. IOP Publishing, 2017.

[6] Hull, Derek, and T. W. Clyne. *An introduction to composite materials*. Cambridge university press, 1996.

[7] Mohamed, Mansour H., and Kyle K. Wetzel. "3D woven carbon/glass hybrid spar cap for wind turbine rotor blade." *Journal of Solar Energy Engineering*128.4 (2006): 562-573.

[8] Hull, Derek, and T. W. Clyne. *An introduction to composite materials*. Cambridge university press, 1996.

[9] Akato, Kokouvi. *"Pretreatment and pyrolysis of rayon-based precursor for carbon fibers."* (2012).

[10] INTRO TO CARBON FIBER. (n.d.). Retrieved from http://www.protechcomposites.com/content/CarbonFiberBasicsWhitePaper.pdf

[11] Fitzer, E., and W. Huttner. "Structure and strength of carbon/carbon composites." *Journal of Physics D: Applied Physics* 14.3 (1981): 347.

[12] THERMOPLASTICS VS THERMOSETTING PLASTICS. (2014). Retrieved from http://www.recycledplastic.com/index.html%3Fp=10288.html

[13] Liu, Yue, Bernd Zwingmann, and Mike Schlaich. "Carbon Fiber Reinforced Polymer for Cable Structures—A Review." *Polymers* 7.10 (2015): 2078-2099.

[14] Wu, Xiang-Fa, and Alexander L. Yarin. "Recent progress in interfacial toughening and damage self-healing of polymer composites based on electrospun and solution-blown nanofibers: An overview." *Journal of applied polymer science* 130.4 (2013): 2225-2237.

[15] Yoon, Sang-Jae, et al. "AE analysis of delamination crack propagation in carbon fiber-reinforced polymer materials." *Journal of Mechanical Science and Technology* 29.1 (2015): 17-21.

[16] Kuwata, M., and P. J. Hogg. "Interlaminar toughness of interleaved CFRP using non-woven veils: Part 1. Mode-I testing." *Composites Part A: Applied Science and Manufacturing* 42.10 (2011): 1551-1559.

[17] Tiwari, S., and J. Bijwe. "Surface treatment of carbon fibers-a review." *Procedia Technology* 14 (2014): 505-512.

[18] Sun, Xiaochen, et al. "Experimental and numerical analysis on Mode-I delamination of CFRP laminates toughened by polyamide non-woven fabric layer." *Materials and Structures* 49.4 (2016): 1191-1200.

[19] Groleau, M. R., et al. "Mode II fracture of composites interlayered with nylon particles." *Composites science and technology* 56.11 (1996): 1223-1240.

[20] Zeng, Shangying, Mark Hoisington, and James C. Seferis. "Particulate interlayer toughening of dicyanate matrix composites." *Polymer composites* 14.6 (1993): 458-466.

[21] Li, L., P. Lee-Sullivan, and K. M. Liew. "The influence of thermoplastic film interleaving on the interlaminar shear strength and mode I fracture of laminated composites." *TRANSACTIONS-AMERICAN SOCIETY OF MECHANICAL ENGINEERS JOURNAL OF ENGINEERING MATERIALS AND TECHNOLOGY* 118 (1996): 302-309.

[22] Jiang, Wei, et al. "Interlaminar fracture properties of carbon fibre/epoxy matrix composites interleaved with polyethylene terephthalate (PET) films." *Polymers and Polymer Composites* 9.2 (2001): 141-146.

[23] Saghafi, Hamed, et al. "The effect of interleaved composite nanofibrous mats on delamination behavior of polymeric composite materials." *Composite Structures* 109 (2014): 41-47.

[24] Arai, Masahiro, et al. "Mode I and mode II interlaminar fracture toughness of CFRP laminates toughened by carbon nanofiber interlayer." Composites Science and Technology 68.2 (2008): 516-525.

[25] Bhanushali, Hardik, and Philip D. Bradford. "Woven glass fiber composites with aligned carbon nanotube sheet interlayers." *Journal of Nanomaterials*2016 (2016): 55.

[26] Zhang, Jin, et al. "Phase morphology of nanofibre interlayers: critical factor for toughening carbon/epoxy composites." *Composites science and technology* 72.2 (2012): 256-262.

[27] Daelemans, Lode, et al. "Nanofibre bridging as a toughening mechanism in carbon/epoxy composite laminates interleaved with electrospun polyamide nanofibrous veils." *Composites Science and Technology* 117 (2015): 244-256.

[28] Bovicelli, F., et al. "On consideration the mode I fracture response of CFRP composite interleaved by composite nanofibers." *Procedia Materials Science* 3 (2014): 1316-1321.

[29] Saghafi, H., et al. "Impact response of glass/epoxy laminate interleaved with nanofibrous mats." *Engineering Solid Mechanics* 1.3 (2013): 85-90.

[30] Li, Gang, et al. "Novel carbon fiber/epoxy composite toughened by electrospun polysulfone nanofibers." *Materials Letters* 62.3 (2008): 511-514.

[31] Zhang, Jin, Tong Lin, and Xungai Wang. "Electrospun nanofibre toughened carbon/epoxy composites: Effects of polyetherketone cardo (PEK-C) nanofibre diameter and interlayer thickness." *Composites science and technology* 70.11 (2010): 1660-1666.

[32] Palazzetti, Roberto, et al. "Influence of electrospun Nylon 6, 6 nanofibrous mats on the interlaminar properties of Gr–epoxy composite laminates." *Composite structures* 94.2 (2012): 571-579.

[33] Khan, Shafi Ullah, and Jang-Kyo Kim. "Improved interlaminar shear properties of multiscale carbon fiber composites with bucky paper interleaves made from carbon nanofibers." *Carbon* 50.14 (2012): 5265-5277.

[34] Sihn, Sangwook, et al. "Improvement of damage resistance in laminated composites with electrospun nano-interlayers." *Composites Science and Technology* 68.3 (2008): 673-683.

[35] Huang, Zheng-Ming, et al. "A review on polymer nanofibers by electrospinning and their applications in nanocomposites." *Composites science and technology* 63.15 (2003): 2223-2253.

[36] Stahl, James J., Alexander E. Bogdanovich, and Philip D. Bradford. "Carbon nanotube shear-pressed sheet interleaves for Mode I interlaminar fracture toughness enhancement." *Composites Part A: Applied Science and Manufacturing* 80 (2016): 127-137.

[37] Greiner, Andreas, and Joachim H. Wendorff. "Electrospinning: a fascinating method for the preparation of ultrathin fibers." *Angewandte Chemie International Edition* 46.30 (2007): 5670-5703.

[38] Casper, Cheryl L., et al. "Controlling surface morphology of electrospun polystyrene fibers: effect of humidity and molecular weight in the electrospinning process." *Macromolecules* 37.2 (2004): 573-578.

[39] Lee, K. H., et al. "Characterization of nano-structured poly (ε-caprolactone) nonwoven mats via electrospinning." *Polymer* 44.4 (2003): 1287-1294.

[40] Hohman, Moses M., et al. "Electrospinning and electrically forced jets. I. Stability theory." *Physics of Fluids (1994-present)* 13.8 (2001): 2201-2220.

[41] Yarin, Alexander L., Sureeporn Koombhongse, and Darrell Hyson Reneker. "Taylor cone and jetting from liquid droplets in electrospinning of nanofibers." *Journal of applied physics* 90.9 (2001): 4836-4846.

[42] Pourdehyhimi, B., et al. "Measuring fiber orientation in nonwovens part V: real webs." *Textile Research Journal* 69.3 (1999): 185-192.

[43] Russell, Stephen J., ed. *Handbook of nonwovens*. Woodhead Publishing, 2006.

[44] Thompson, C. J., et al. "Effects of parameters on nanofiber diameter determined from electrospinning model." *Polymer* 48.23 (2007): 6913-6922.

[45] Falcone, James S. "Silicon Compounds: Anthropogenic Silicas and Silicates." *Kirk-Othmer Encyclopedia of Chemical Technology* (2005).

[46] Xu, Bugao. "Measurement of pore characteristics in nonwoven fabrics using image analysis." *Clothing and Textiles Research Journal* 14.1 (1996): 81-88.

[47] Xie, Jiangbing, and You-Lo Hsieh. "Ultra-high surface fibrous membranes from electrospinning of natural proteins: casein and lipase enzyme." *Journal of Materials Science* 38.10 (2003): 2125-2133.

[48] Deitzel, J. M., et al. "The effect of processing variables on the morphology of electrospun nanofibers and textiles." *Polymer* 42.1 (2001): 261-272.

[49] Fridrikh, Sergey V., et al. "Controlling the fiber diameter during electrospinning." *Physical review letters* 90.14 (2003): 144502.

[50] Pakuła, T., J. Grebowicz, and M. Kryszewski. "The kinetics of spontaneous changes in the phase structure of molten two-component polymer systems." *Polymer Bulletin* 2.12 (1980): 799-804.

[51] Tan, S. H., et al. "Systematic parameter study for ultra-fine fiber fabrication via electrospinning process." *Polymer* 46.16 (2005): 6128-6134.

[52] Jacobs, Valencia, Rajesh D. Anandjiwala, and Malik Maaza. "The influence of electrospinning parameters on the structural morphology and diameter of

electrospun nanofibers." *Journal of Applied Polymer Science* 115.5 (2010): 3130-3136.

[53] Theron, S. A., E. Zussman, and A. L. Yarin. "Experimental investigation of the governing parameters in the electrospinning of polymer solutions." *Polymer*45.6 (2004): 2017-2030.

[54] Demir, Mustafa Muammer, et al. "Electrospinning of polyurethane fibers."*Polymer* 43.11 (2002): 3303-3309.

[55] Jarusuwannapoom, Teeradech, et al. "Effect of solvents on electro-spinnability of polystyrene solutions and morphological appearance of resulting electrospun polystyrene fibers." *European Polymer Journal* 41.3 (2005): 409-421.

[56] Zuo, Weiwei, et al. "Experimental study on relationship between jet instability and formation of beaded fibers during electrospinning." *Polymer Engineering & Science* 45.5 (2005): 704-709.

[57] Cui, Wenguo, Yue Zhou, and Jiang Chang. "Electrospun nanofibrous materials for tissue engineering and drug delivery." *Science and Technology of Advanced Materials* (2016).

[58] Baji, Avinash, et al. "Electrospinning of polymer nanofibers: effects on oriented morphology, structures and tensile properties." *Composites science and technology* 70.5 (2010): 703-718.

[59] Lee, Keun Hyung, et al. "Influence of a mixing solvent with tetrahydrofuran and N,N-dimethylformamide on electrospun poly (vinyl chloride) nonwoven mats." *Journal of polymer science part B: polymer physics* 40.19 (2002): 2259-2268.

[60] Fennessey, Sian F., and Richard J. Farris. "Fabrication of aligned and molecularly oriented electrospun polyacrylonitrile nanofibers and the mechanical behavior of their twisted yarns." *Polymer* 45.12 (2004): 4217-4225.

[61] Fong, H., I. Chun, and D. H. Reneker. "Beaded nanofibers formed during electrospinning." *Polymer* 40.16 (1999): 4585-4592.

[62] Liu, Yong, et al. "Controlling numbers and sizes of beads in electrospun nanofibers." *Polymer International* 57.4 (2008): 632-636.

[63] Megelski, Silke, et al. "Micro-and nanostructured surface morphology on electrospun polymer fibers." *Macromolecules* 35.22 (2002): 8456-8466.

[64] Lee, K. H., et al. "The change of bead morphology formed on electrospun polystyrene fibers." *Polymer* 44.14 (2003): 4029-4034.

[65] Lin, Tong, et al. "The charge effect of cationic surfactants on the elimination of fibre beads in the electrospinning of polystyrene." *Nanotechnology* 15.9 (2004): 1375.

[66] Yang, Dayong, et al. "Fabrication of aligned fibrous arrays by magnetic electrospinning." *Advanced Materials* 19.21 (2007): 3702-3706.

[67] Kim, GeunHyung, and WanDoo Kim. "Formation of oriented nanofibers using electrospinning." *Applied physics letters* 88.23 (2006): 233101.

[68] De Vrieze, Sander, et al. "The effect of temperature and humidity on electrospinning." *Journal of materials science* 44.5 (2009): 1357.

[69] Zheng, Nan, et al. "Improvement of interlaminar fracture toughness in carbon fiber/epoxy composites with carbon nanotubes/polysulfone interleaves." *Composites Science and Technology* 140 (2017): 8-15.

CHAPTER 3 EXPERIMENTS

3.1 Electrospinning

3.1.1 Raw Materials

Poly(vinyl alcohol) (PVA) and poly(vinyl acetate) (PVAc), acetic acid (Table 3.1) were purchased from Sigma-Aldrich.

Table 3.1 Summary for electrospinning materials

Polymer	Chemical Formula	Chemical Structure	Molecular Weight (Mn)	Solvent
Poly(vinyl alcohol)	$(C_2H_4O)n$	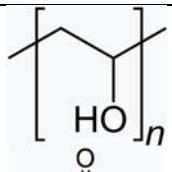	130,000	Water
Poly(vinyl acetate)	$(C_4H_6O_2)n$	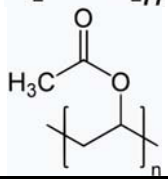	100,000	Acetic acid and water

3.1.2 Dope Preparation

PVA was dissolved in deionized water at 600 RPM and ~80 °C for 30 min to attain clear spinning dopes. Dopes were conditioned at room temperature for at least 1 h. PVAc was dissolved in acetic acid and deionized water at 3:1 ratio over night with stirring at room temperature until the solution turned clear.

3.1.3 Electrospinning Process

Electrospinning was performed using the setup zhown in Figure 3.1. The electrospinning set-up comprised of a syringe pump, 10 mL syringe, high voltage supply and rotating drum (70 cm in circumference and 36 cm in width). The maximum linear velocity of the rotating collector was 1.12 m/s (96 rpm). The minimum linear velocity of

the rotating collector was 0.058 m/s for stable rotation without shaking. The flow rate for the syringe (having a 12-mm inner diameter) was varied. Positive charge was applied to the tip of the needle. The collector was grounded. Under high voltage, fibers deposited onto the collector.

Figure 3.1 Electrospinning equipment with rotating drum

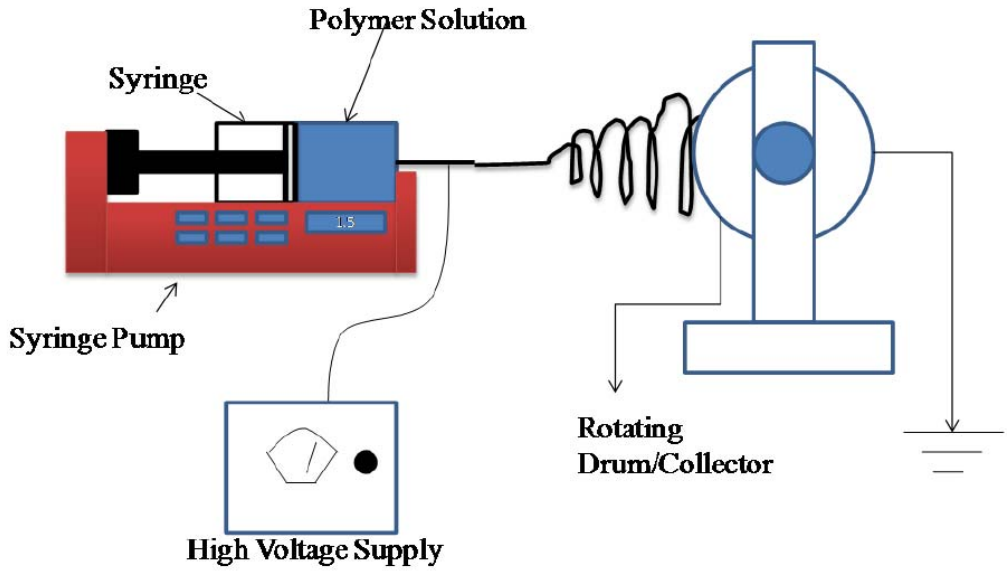

Figure 3.2 Scheme of electrospinning set up with rotating drum

3.1.4 Scanning Electron Microscope (SEM)

The morphology of the electrospun fibers was observed under Field Emission SEM (FEI Verios 460L). Samples were sputter coated with Au/Pa. All the images were taken 1, 5, and 25 kX using 5 kV accelerating voltage.

3.1.5 Diameter Measurement by ImageJ

Images analyzed by ImageJ, were used to record 50 measurements of fiber diameter from the 25 kX magnified webs. Raw data of diameters were saved in Microsoft Excel. Processed data (such as the average, maximum, minimum, standard deviation and histogram of fiber diameters were calculated for further analysis.

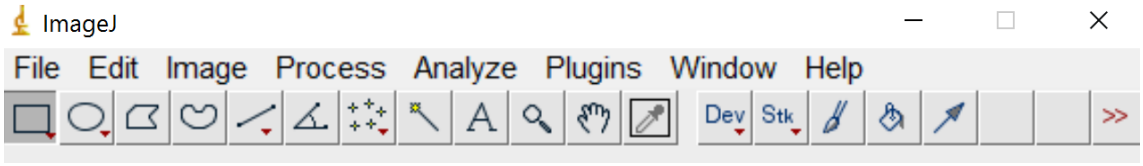

Figure 3.3 Tool interface of ImageJ

3.1.6 Fiber Orientation Characterized by MATLAB

Orientation distribution was described by histograms, dominate angle, $\langle \cos^2\varphi \rangle$, and Ht. Fiber orientation of different webs was characterized by the Herman's orientation factor (Ht) in Equation 2.1. MATLAB programming was used to solve for $\langle \cos^2\varphi \rangle$ from the orientation distribution function. The MATLAB code is in the Appendix I [2]. SEM images at 5 kX magnification were processed. The reference angle was 0°; the horizontal direction.

3.2 Carbon Fiber Reinforced Plastics (CFRP)

3.2.1 Fabrication of CFRPs with Electrospun Interlayers

Carbon fabrics were purchased from Elite Motoring; see details in Table 3.2. Fibers were electrospun directly on carbon fabric. The interlayer was set in the middle of CFRPs.

Table 3.2 The Specification of Carbon Fabric

Weave	End/Picks per inch	Yarn size (warp/weft)	Basis weight
Plain weave	12.5	3k	193.26 gsm

Composites were fabricated by vacuum assisted resin transfer molding (VARTM). The stacking sequence of carbon fabric was in one direction, as $[0]_n$. Here "n" represents the number of layers. A release film was placed at the bottom of woven carbon fabrics. On the top of carbon fiber reinforcement was woven nylon- as peel ply layer that could ensure even resin distribution during processing. Resin flow media was laid on top of the peel ply layer. It allowed even resin flow rapidly across the preform. Nylon bagging film was sealed by tape. A negative pressure of 100 kPa was applied during VARTM for the vacuum. Epoxy resin 2120 and epoxy hardener 2000 were blended at 100:27.

Mixed resin was degassed in a vacuum desiccator for 30 min to remove air bubbles. Subsequently, the mixture of resin and hardener were injected into the mold under vacuum pump. Composites cured at room temperature for at least 24 hours.

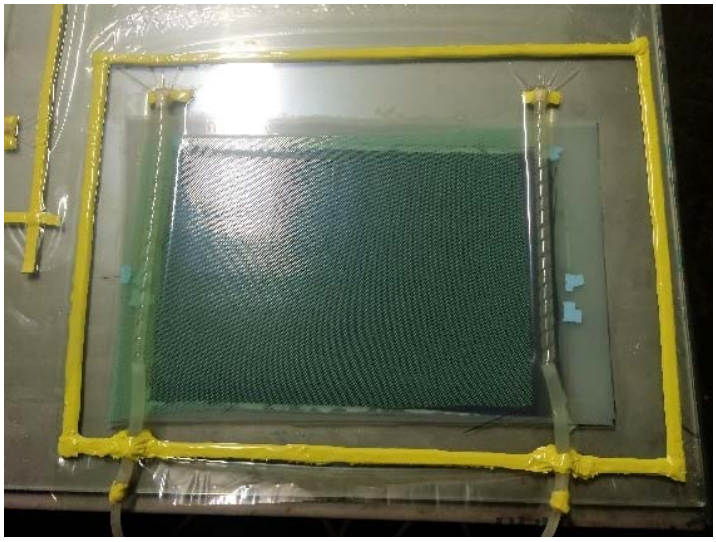

Figure 3.4 Fabrication of CFRP with the vacuum assisted resin transfer modeling in the laboratory scale

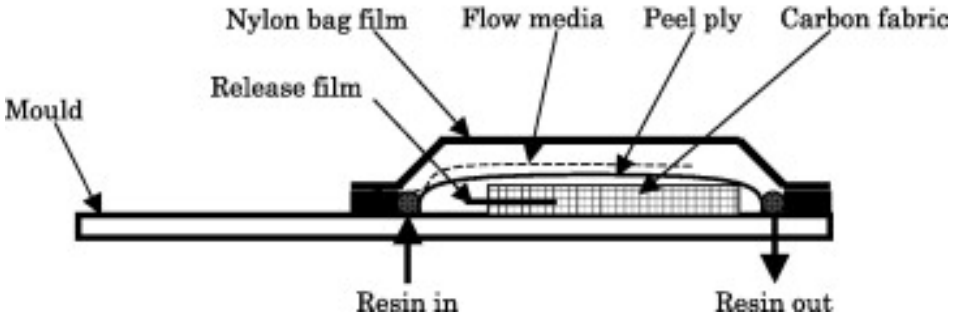

Figure 3.5 Schematic diagrams of CFRP fabrication with the vacuum assisted resin transfer modeling [3]

3.2.2 Interlaminar Shear Test

The interlaminar shear test was carried out based on AMTS D5869 that was lap shear adhesion for fiber reinforced plastics bonding. Compared to the normal delamination test system like double cantilever beam test as well as end notched flexure test, the lap shear adhesion test was more straightforward and easy to operate. However, the fabrication of samples is more challenging with the vacuum assisted resin transfer modeling which is discussed later. MTS landmark servohydraulic test systems interfaced with laser extensometer (Figure 3.6) was used. The test speed was 13 mm/min as required by the standard.

Figure 3.6 MTS Landmark Servohydraulic Test Systems available in the Composite Core Facility, College of Textiles, NC State University.

3.2.3 Characterization of Fracture Surface by Confocal Microscope

The fracture surface of CFRPs was characterized with laser scanning confocal microscopy (Olympus LEXT 4000). Images were scanned at 50 X for 2-D images and 100 X for 3D images.

Figure 3.7 Olympus LEXT 4000 confocal microscopy available in the Chemistry Lab, College of Textiles, NC State University.

References

[1] Gluck, Jessica Marie. "Electrospun Poly (e-caprolactone)(PCL) Nanofibrous Scaffolds for Liver Tissue Engineering." (2007).

[2] Chun-kui, J. I. N. "Orientation analysis of electrospun nanofibers based on electron microscopy image [J]." *Silk* 9 (2011): 005.

[3] Kuwata, M., and P. J. Hogg. "Interlaminar toughness of interleaved CFRP using non-woven veils: Part 1. Mode-I testing." *Composites Part A: Applied Science and Manufacturing* 42.10 (2011): 1551-1559.

[4] Pourdehyhimi, B., et al. "Measuring fiber orientation in nonwovens part V: real webs." *Textile Research Journal* 69.3 (1999): 185-192.

[5] Russell, Stephen J., ed. *Handbook of nonwovens*. Woodhead Publishing, 2006.

APPENDIX A.Customized Code to Characterize the Orientation of Fibers [2]

```
clear all

PS = imread('Imge name'); % Read the color image file

%I1 = PS; % Read the BMP greyscale image file

I1 = rgb2gray(PS); % Transfer into a grayscale image

I2 = wiener2(I1,[2,2]); % Remove noise

I3 = imadjust(I2); % Adjust the grayscale image

I4 = medfilt2(I3); % Two-dimensional median filter

I5=imbinarize(I4,'adaptive'); % Binarization

I6 = bwlabel(I5); % Mark the binary image

STATS = regionprops(I6,'Area'); % Statistics of the total number of pixels in each region

idx1 = find([STATS.Area]>20); % Filter the highlights area where the pixel is greater
than 20

I7 = ismember(I6,idx1); % Remove the smaller area

imshow(I7); % Show image

I8=bwlabel(I7); %Re-mark the binary image

L=regionprops(I8,'Orientation'); % Find orientation angles in the image

for i = 1:length(L)

   vector(i) = L(i).Orientation;

end; % Read angles one by one in the data base

for i = 1:length(L)

   vector(i) = round(L(i).Orientation);
```

```
end % Round the orientation angles to nearest integer
A=unique(vector); %Pick up all the angles in the orientation data base
n = histc(vector,A); % Count the number of fiber angles measured
f = n/sum(n); % Sum of the number of fiber angles measured
Ht_min=2; % Give an initial value to Ht_min
Rotate_Angle=0; % Give an initial value to Rotate_Angle
for j=0:180
   sum_AR = sum(cos((A+j)/180*pi).^2.*f);
   Ht = 2*sum_AR-1; % Calculation of Ht value by every 1˚rotation
   if Ht<Ht_min
      Ht_min=Ht;
      Rotate_Angle=j;
   end % Find the minimized Ht value and record it as well as the rotating angle
end
Concentrated_Angle = 90-Rotate_Angle;
if Concentrated_Angle < 0
   Concentrated_Angle=Concentrated_Angle+180;
End % Calculation of dominated angle
for k=1:length(L)
   if vector(k) < 0
      vector(k)=vector(k)+180;
   end
```

```
end % Make sure all the angles within 0˚ to 180˚

Concentrated_Angle % Output dominated angle

Ht_min % Output minimized Ht value

figure(2), histogram(vector,9,'Normalization','probability'); % Draw the histogram

xlabel('Angle'); % Set label to x axis of histogram

ylabel('Frequence'); % Set label to y axis of histogram
```

CHAPTER 4 RESULTS AND DISCUSSIONS

4.1 The Effect of Electrospinning Parameters on web structure

4.1.1 The Effect of Concentration

PVA is hydrophilic because of its pendant hydroxyl groups. Water was chosen as the solvent for PVA dopes. Electrospinning parameters for hydrolyzed PVA are shown in Table 4.1. SEM images in Figure 4.1 show 10% PVA was too low. Beads were generated along electrospun fibers. To eliminate beads, the PVA concentration was increased to 12%. At 12% PVA, suspended polymer solution stuck to the tip of the needle at higher flow rates. Flow rate was decreased to 0.5 ml/h and applied voltage was set to 25 kV to maintain a stable Taylor cone. SEM images are in Figure 4.1. Optimized electrospinning parameters are shown in Table 4.2. It was apparent that beads did not form. Uniform fibers that cylindrical in nature were collected.

Table 4.1 Electrospinning parameters of first trial of eletrospun PVA

Concentration (%)	Voltage (KV)	Flow Rate (ml/h)	Tip to collector distance (cm)	Rotating speed (m/s)	Collection Time (h)
10	15	1	12	1.12	1

Table 4.2 Optimized electrospinning parameters for electrospun PVA

Concentration (%)	Voltage (KV)	Flow Rate (ml/h)	Tip to collector distance (cm)	Collection Time (h)
12	25	0.5	12	1

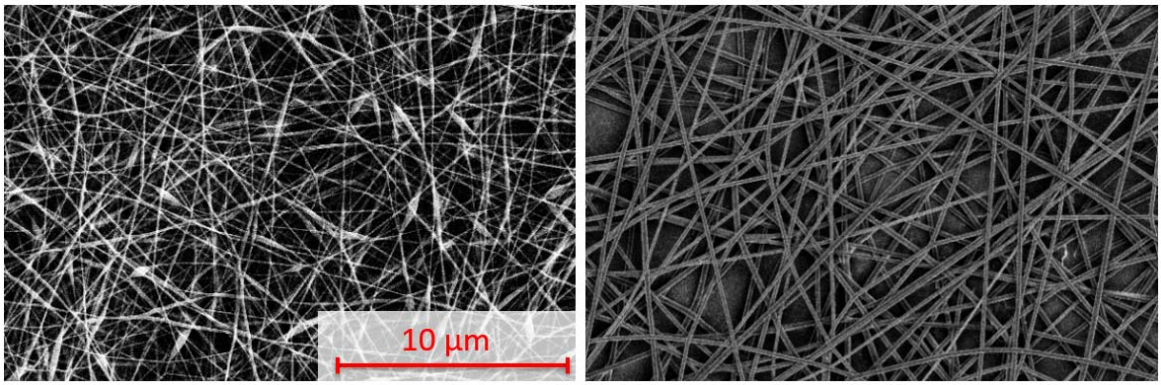

Figure 4.1 SEM images at 5k of electrospun PVA with the first trail electrospinning parameters (left) and with optimized electrospinning parameters (right)

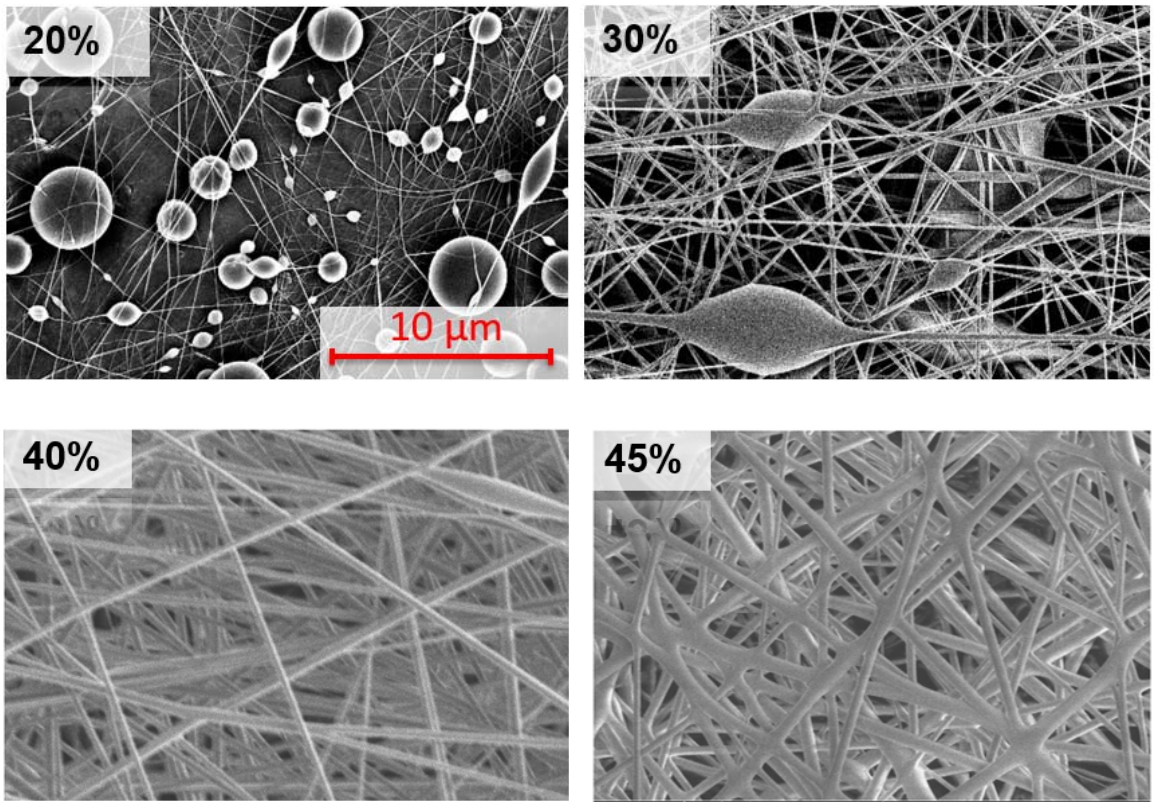

Figure 4.2 SEM images at 5k for PVAc with different concentration

PVAc is the hydrophobic polymer that is soluble in acetic acid, a polar solvent of similar chemistry [4]. PVAc and acetic acid both have acetate groups. The PVAc solvent system comprised acetic acid and water at 3:1. Water was added for economical and environmental considerations [5]. PVAc dope was less viscose than PVA dope at the sample polymer concentration. Keeping other electrospinning parameters constant, PVAc content was increased to 20-45%. SEM images of the nanofibers are shown in Figure 4.2. Fiber size is represented in Figure 4.3. At higher concentration, the number of beads decreased, even as polymer concentration increased to 45%. From low to higher concentrations, bead shape evolved from spheres to spindle. Finally, these could not be found among uniform fibers. Average fiber diameter and diameter distribution were not significantly affected by concentration increases, except at 45% PVAc.

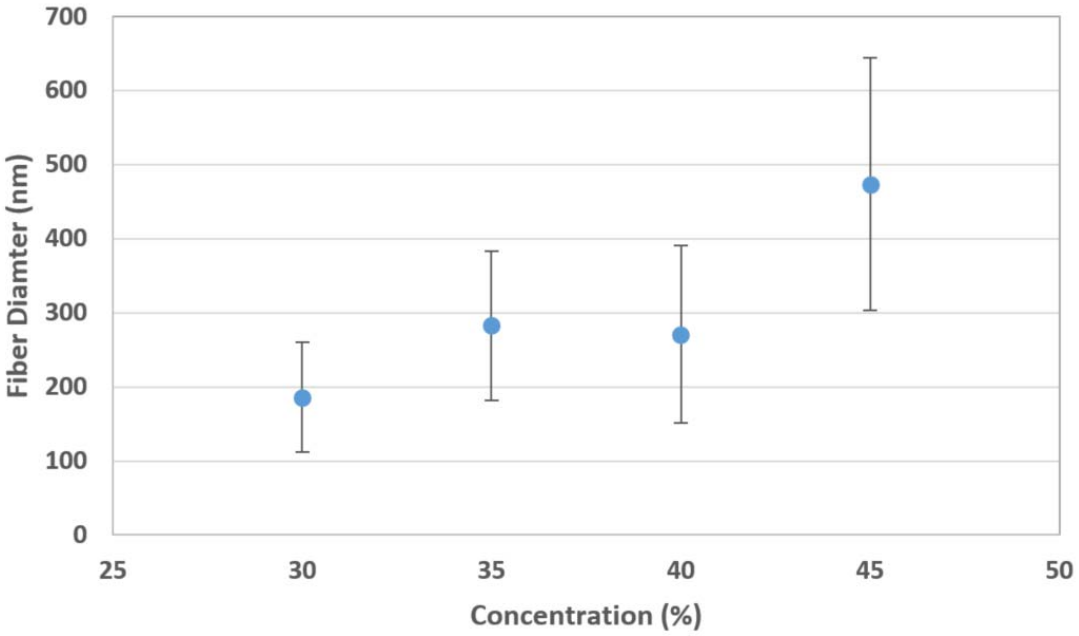

Figure 4.3 Effect of concentration on PVAc fiber diameter

At the same volume, the beads have less surface than fiber geometries. The larger surface area has the potential to improve surficial contact between electrospun nanofibers and matrix resin. Surface area is therefore important for the wettability of electrospun fibers by matrix resin. Ideally nanofiber uniformity permits the even distribution of stress; such that electrospun fibers should bridge cracked matrix resin. Thus, the elimination of beads is thought to be significant for CFRP toughening.

4.1.2 The Effect of Collector Surface Velocity

In this study, the collector was the rotating drum. Take velocities by the collector were studied to understand the influence of drum velocity on web structure (see Table 4.3). SEM images of electrospun nanofibers are shown in Figure 4.4 and Figure 4.5. These figures indicate the diameter of PVAc nanofibers were larger in size than PVA nanofibers. Their fiber diameter distribution was also larger. The increase of the surface velocity resulted in thinner PVA fibers, but there was no effect on electrospun PVAc. PVA fibers

that were collected at 1.12 m/s had a Ht value of 0.41. Using the higher rotation speed did not affect the orientation of PVAc fibers.

Table 4.3 Plan of electrospinning parameters to study the effect of drum surface speed on web structure

Polymer	Concentration (%)	Voltage (Kv)	Flow Rate (ml/h)	Tip to Collector Distance (cm)	Collection Time (hr)	Drum surface speed (m/s)
PVA	12	25	0.5	12	1	1.12/0.058
PVAc	40					

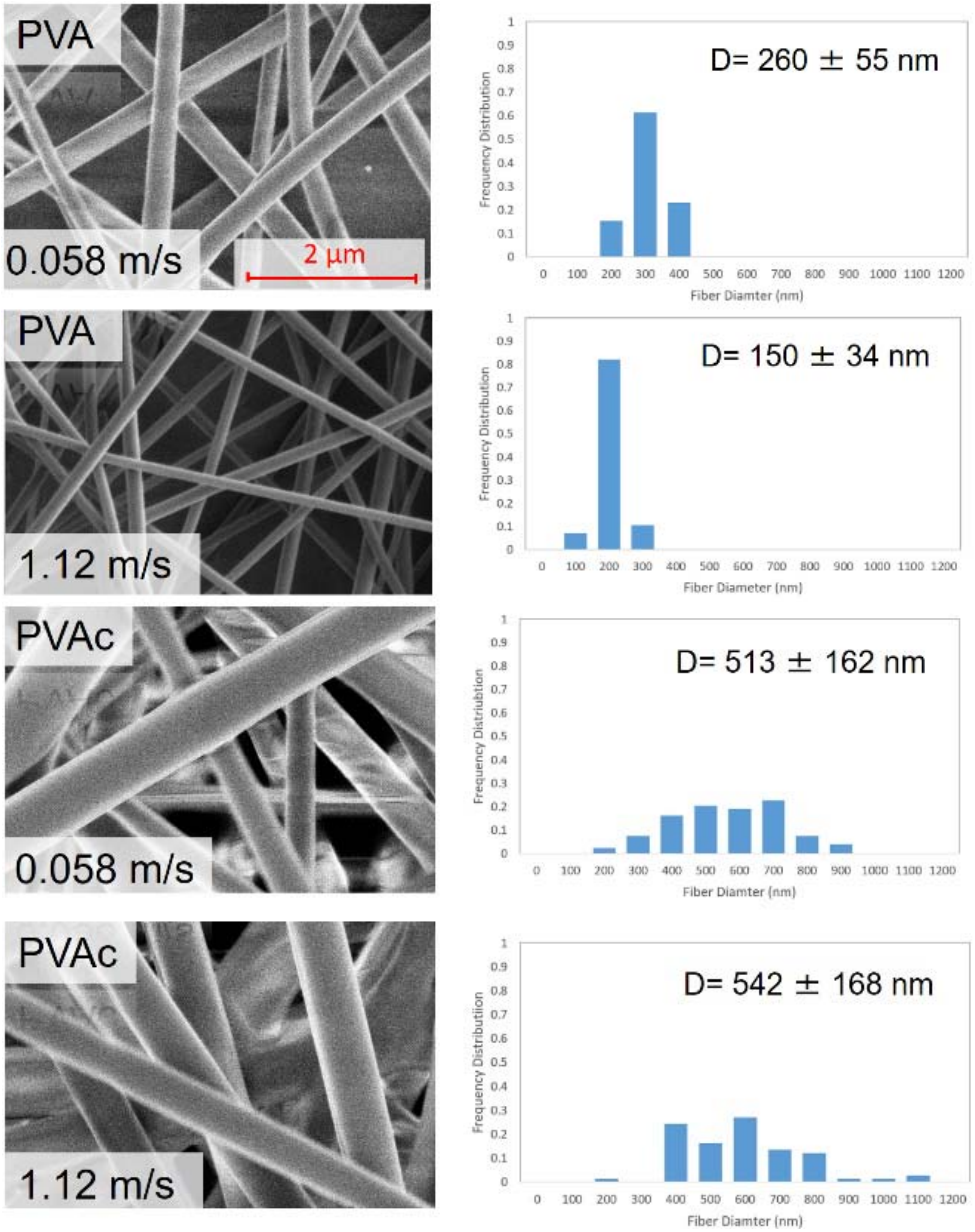

Figure 4.4 SEM images at 25k and fiber diameter distribution histograms with the fiber diameter displayed on the top right corner

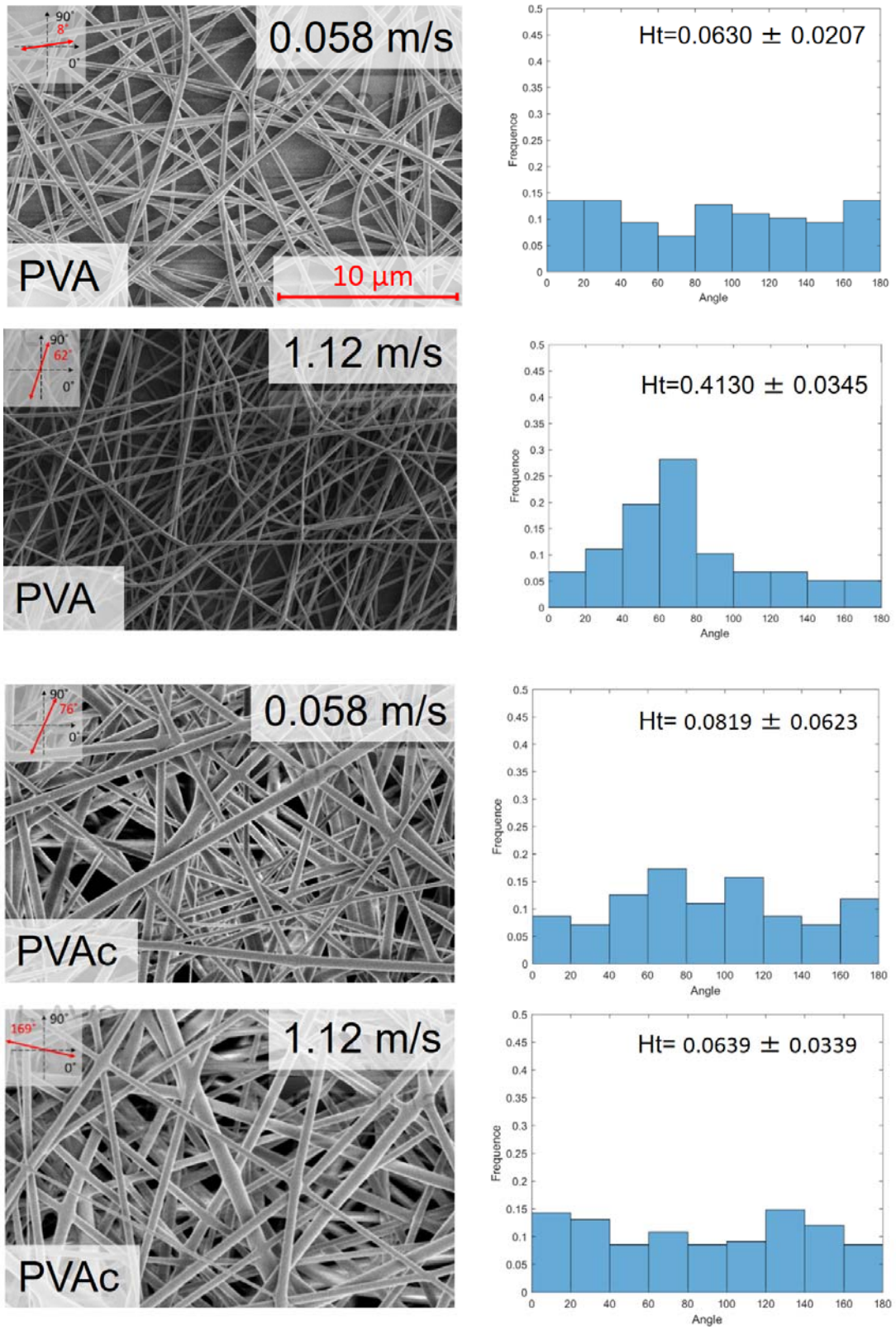

Figure 4.5 SEM images at 5k and fiber orientation distribution histograms with the Ht values displayed on the top right corner

4.1.3 The Effect of the Tip to Collector Distance

The electrospinning parameters of PVA and PVAc were similar except for differences in polymer concentration. TCD was varied from 6-16 cm, as listed in Table 4.4. As shown in Figure 4.6 and Figure 4.7, TCD had minor impact on fiber diameter and orientation distribution. Changes in solvent evaporation from fiber webs were evident among SEM images (Figure 4.8). Beads formed when the TCD equaled 12 cm for electrospun PVAc.

Table 4.4 Plan of electrospinning parameters to study the effect of TCD on web structure

Polymer	TCD (cm)
PVA (12% in concentration, 25 Kv in voltage, 0.5 ml in flow rate, 1 hr in collection time, 1.12 m/s in rotation speed)	6, 8, 10, 12, 14, 16
PVAc (40% in concentration, 25 Kv in voltage, 0.5 ml in flow rate, 1 hr in collection time, 1.12 m/s in rotation speed)	

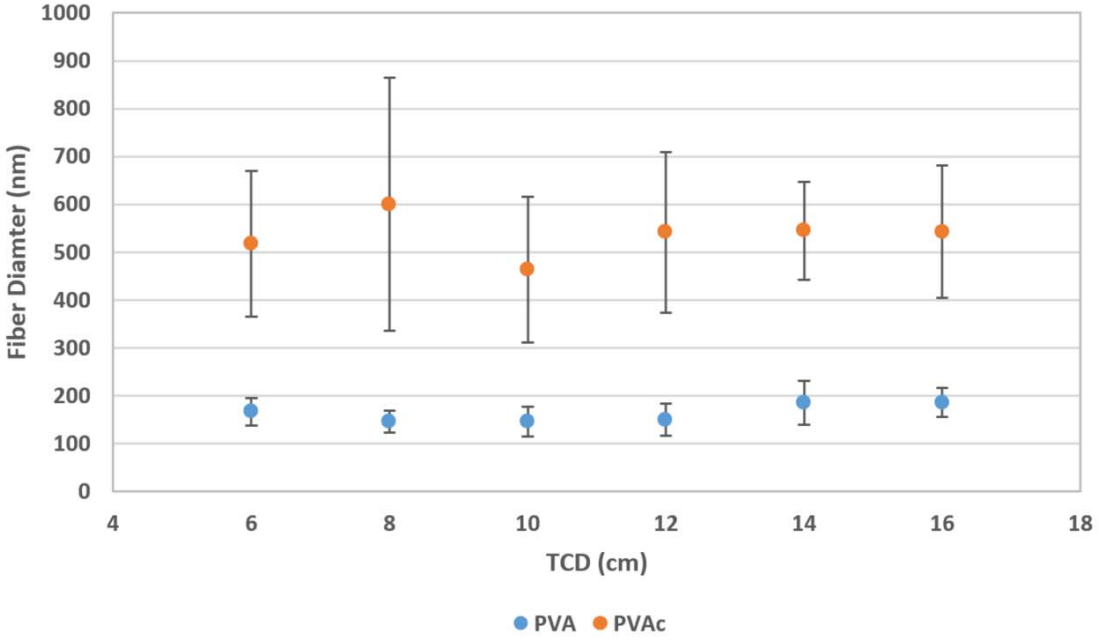

Figure 4.6 The effect of TCD on fiber diameter

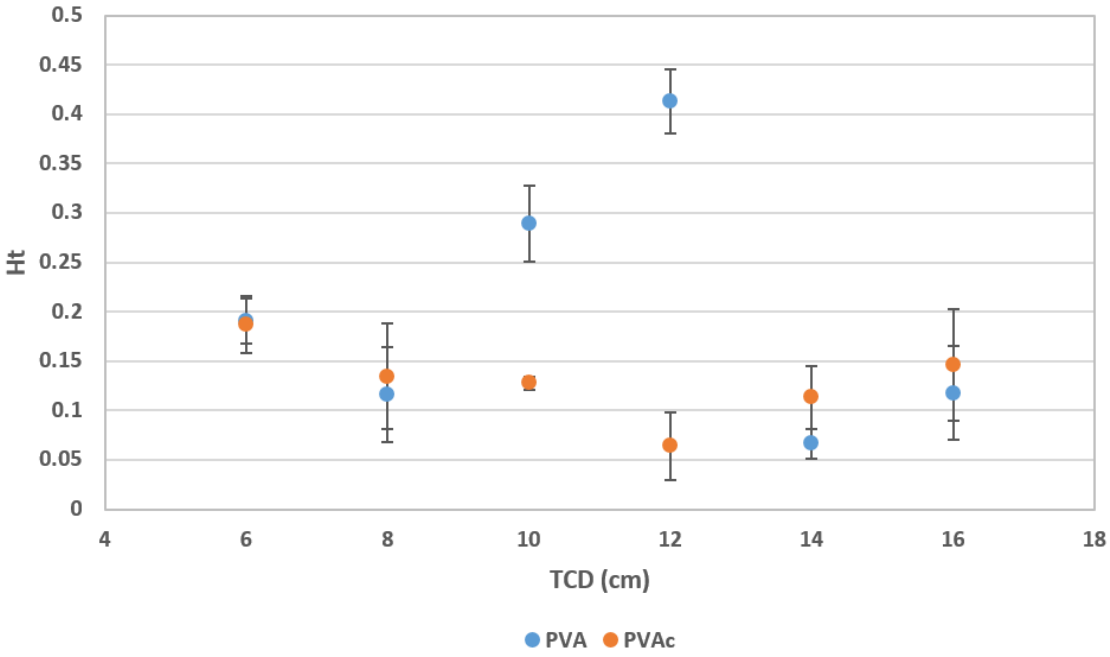

Figure 4.7 The effect of TCD on fiber orientation

TCD effects on nanofibers are caused by changes in electric field strength and flight from the tip to collector [9][10][11][12]. Under the same applied voltage, the longer TCD values reflect weaker electric field strengths. Whipping and bending under the applied electric field leads to nanoscale fibers. Before the polymer jet completely solidifies, flight time give fibers more opportunity to elongate and result in smaller diameter fibers. TCD did not show any apparent effect on fiber diameter. According to Figure 4.7, changing TCD did not significantly affect the orientation of electrospun PVA and PVAc fibers. Fiber orientation was unaffected by the increase in linear velocity. At TCD=12 cm, PVA webs had a Ht=0.41. At TCD=12 cm, water had totally evaporated from PVA nanofibers. Higher linear drum velocity is needed to align the fibers at TCD=12cm.

Figure 4.8 shows SEM images of PVAc at 1 kX and different TCD lengths. Images revealed the evolution of solvent evaporation from the fibers. As shown in the image, a

few fibers stuck together. At TCD=12 cm, smooth individual fibers were achieved. The longer TCD led to longer flight time, so solvent could completely evaporate. Fibers deposited on the collector were smooth, individual fibers. When TCD was longer than 12 cm, beads were detected along fibers. By weakening electric field, beads had formed at greater lengths. The electrostatic force carried out by the polymer jet was dropped down, succeeding the surface tension took the favorable conditions to form beads.

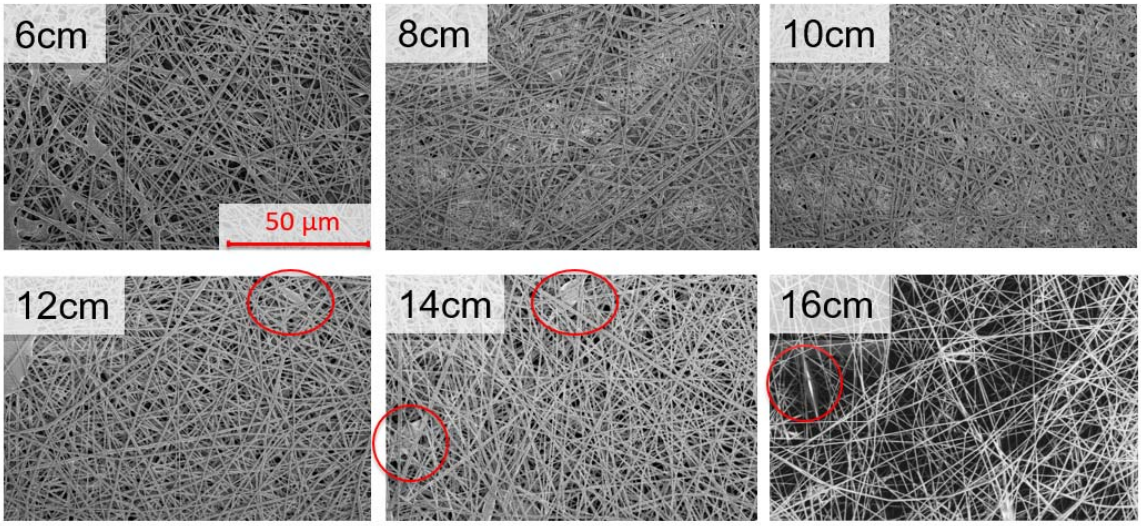

Figure 4.8 SEM images of electrospun PVAc at 1k with different TCD

4.1.4 Summaries and Conclusions

Electrospinning is a fascinating approach to fabricate nanofibers. Varying electrospinning parameters shows the difficulty in controlling web structure. In this study, three important variables were studied: polymer concentration, drum speed, and TCD for the electrospinning of PVA and PVAc. Their effect on web structure (including bead formation, fiber size, and fiber orientation) was studied.

Varying polymer concentration was used to eliminate beads from electrospun fibers. As PVAc concentration increased, beads transformed from spheres to spindle until uniform fibers formed. Bead-free PVA nanofibers formed from dopes of 12% PVA; whereas, bead-

free PVAc nanofibers formed from dopes of 40% PVAc. TCD at 12 cm was found to give Ht=0.41. Longer TCD beyond 12 cm generated beads among fibers, electric field was too weak to yield uniform fibers. All in all, changing electrospinning parameters could also affect differences in web structure. The Effect of Electrospun Interlayers on the CFRP Delamination Resistance

4.1.5 Preliminary Experiment

4.1.5.1 Design of Test Sample

Interlaminar shear testing was performed under ASTM D5868. Two designs for sample fabrication were evaluated (see Figure 4.9). Plan 1 was based on an integrated design. The carbon fabric was treated as the pad to fill the gap underneath the bottom film which was the separator between the sample and table. Carbon fabric could not fit perfectly adjacent to the film layer. During VARTM defects could form during resin transfer molding, as shown in Figure 4.10. Defects would become points of compromise during interlaminar shear testing.

Plan 2 was more complex (as shown in Figure 4.10) but lead to reliable results. The film was inserted into the midplane of the composite. After the fabrication, both sides of the composite were cut to give the same sample shape on each side of the testing specimen.

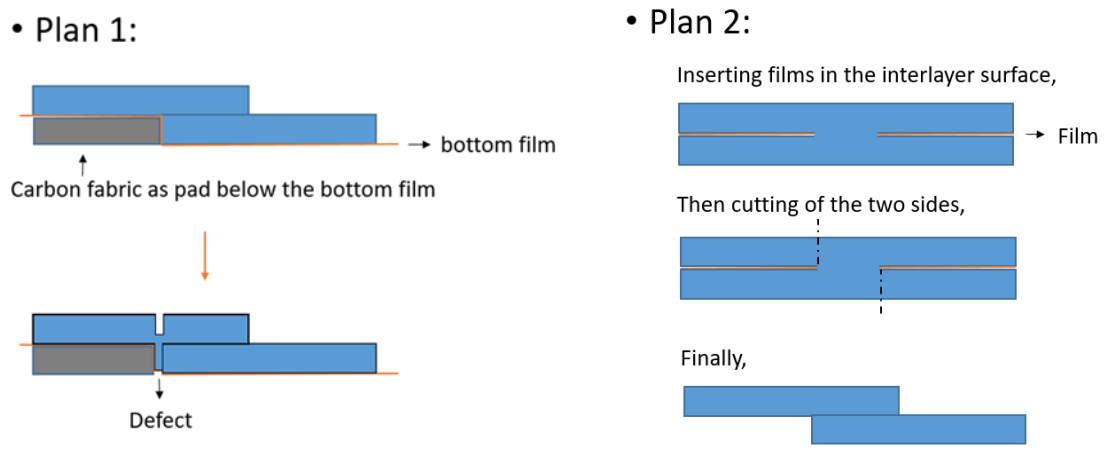

Figure 4.9 Designs of fabrication of CFRP for interlaminar shear test in the cross section

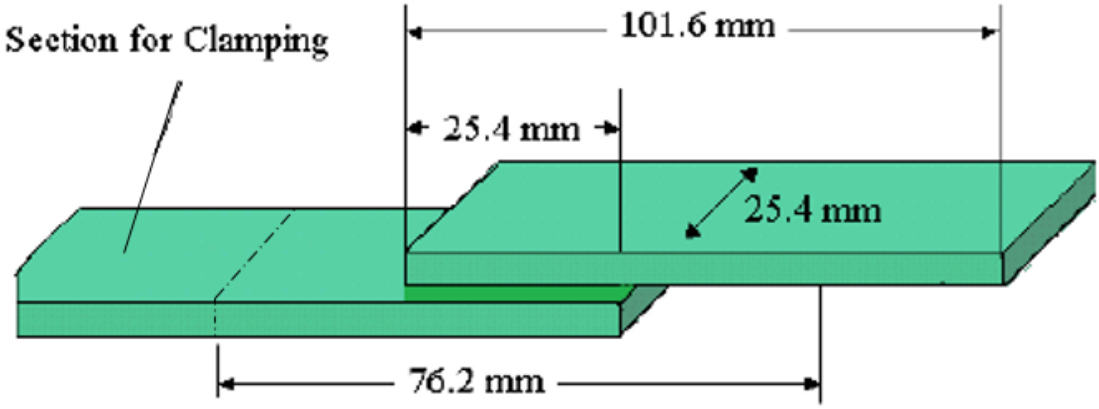

Figure 4.10 Fabrication of sample for interlaminar shear test with specific size

4.1.5.2 Decision of Composites Layers

The control sample without the electrospun interleaves was fabricated starting with two layers. After the interlaminar shear test, the sample was broken at the edge of the overlapping area instead of failing in shear. This denoted the tensile strength of one layer of the layer composite was weaker than the interlaminar shear strength. Data plotted in Figure 4.11. reflected meaningful information. Negative extension at the beginning of the test, as shown in “a” section, revealed an issue with setting the extensometer at zero. The

downside of extension “b” was in response to sample bending, a nonplanar stress. The peak at “c” point was in response to the maximum tensile strength of one CFRP layer.

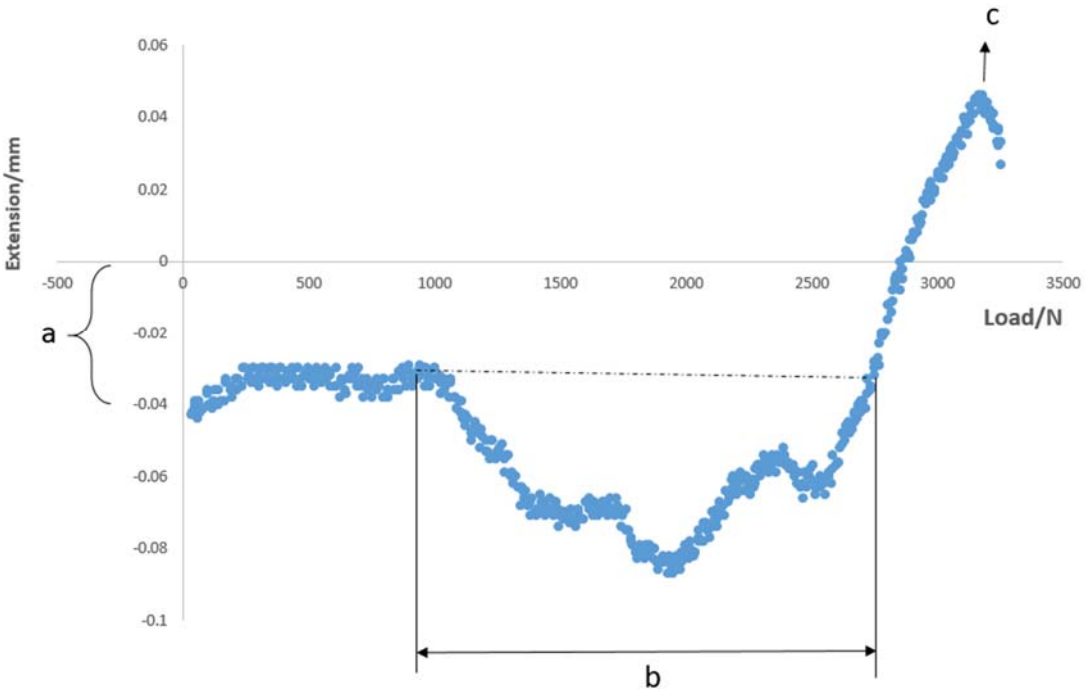

Figure 4.11 The results for interlaminar shear test with 2-layer composites

To avoid the failure mode observed for Plan 1, two extra sheets of woven carbon fabric were stuck to both sides of the sample. Their presence helped to balance force in the same plane. CFRP samples comprised 8 layers (4 layers on each side) to guarantee the tensile strength was higher than the interlaminar shear strength. Completed samples are represented in Figure 4.12. The improved design of for sample manufacturing lead sample fracture in shear mode- while avoiding premature tensile breakage. Besides the control sample, several CFRP samples having electrospun interleaves were testing for differences in delamination resistance. Electrospun interleaves were fabricated with different electrospinning parameters, as shown in Table 4.5.

The polymer volume of 4 ml PVA dope was used. This quantity was based on experience and previous literature. Subsequently, the volume of PVAc dope (1.1 ml) was calculated as being able to yield a similar basis weight when spun onto carbon fabric. The calculations were given in the APPENDIX. Calculation of PVAc. But mass losses during electrospinning led to adjustments in solution volume. 0.88 ml PVAc dope was applied to keep the basis weight of PVA interleaves the same as those spun from PVA. Several basis weights of PVAc web (as shown in Table 4.5) were tested as toughening layers within CFRP.

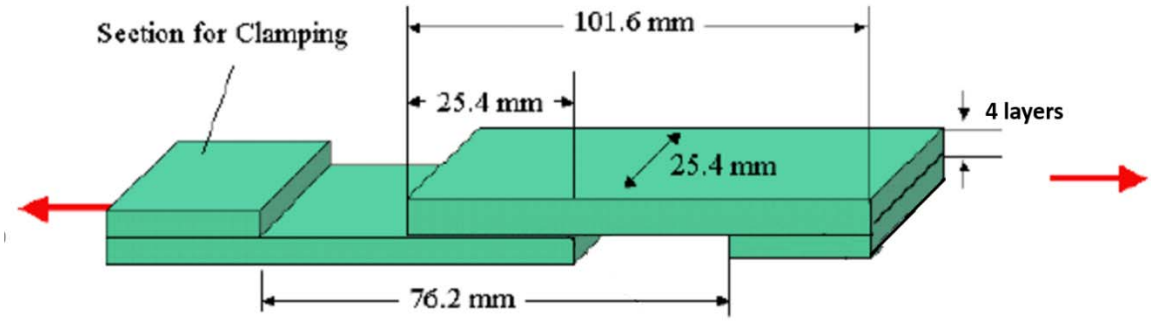

Figure 4.12 CFRP sample manufacture with 8 layers (4 layers each side) with two extra cushions each side. From the top to the bottom are top and left views as well as the schematic of final sample manufacture

Table 4.5 Electrospinning parameters for the electrospun interleaves in the CFRP

Sample	Polymer	Electrospinning Parameters					Polymer Volume (ml)
		Concentration (%)	Surface speed (m/s)	TCD (cm)	Voltage (kV)	Flow Rate (ml/h)	
Control	-	-	-	-	-	-	-
1	PVA	12	0.058	12	25	0.5	4
2			1.12				4
3	PVAc	40					0.88
4							1.1
5							2.2
6							6.6

4.1.6 The Effect of Electrospun Interlayers on the CFRP Delamination Resistance

The data received from shear tests are in Figure 4.6. Ten trials were carried out for each sample. The average and maximum shear stress are reported along with the values of shear strain and toughness. According to data graphs in Figure 4.14, the PVA electrospun interlayer reduced CFRP toughness. Moreover, the electrospun PVA, having

Ht=0.41, greatly reduced maximum shear strain of the composite by 64%; shear stress reduced by 44%; and toughness dropped by 65%. At the same basis weight, CFRP samples of electrospun PVAc had improved shear stress at an increase of 1.3% and toughness was enhanced by 10%.

Since PVAc toughened composites more than PVA, the basis weights of PVAc interleaves were varied for optimal results. With the increase in basis weight for electrospun PVAc interleaves, better toughening was detected without compromising shear strain and shear stress. However, when the PVAc basis weight reached 10 g/m^2, there was not any improvement in toughness.

Table 4.6 The summary of shear test

Sample	Basis weight (g/m2)	Maximum Shear Strain (%)	Maximum Shear Strength (Mpa)	Energy to break (N*mm)
Control	-	0.66 ± 0.12	14.88 ± 0.77	4018.15 ± 440.52
PVA, low speed	4.095	0.36 ± 0.15 (↓ 45.12%)	10.77 ± 0.88 (↓ 27.57%)	2077.23 ± 293.86 (↓ 48.30%)
PVA, high speed	3.985	0.24 ± 0.09 (↓ 64.21%)	8.40 ± 0.84 (↓ 43.51%)	1402.15 ± 287.08 (↓ 65.10%)
PVAc, high speed	3.922	0.45 ± 0.09 (↓ 31.81%)	11.93 ± 1.25 (↓ 19.82%)	3136.41 ± 621.16 (↓ 21.94%)
	5.010	0.62 ± 0.11 (↓ 5.09%)	15.07 ± 1.23 (↑ 1.28%)	4428.31 ± 786.32 (↑ 10.21%)
	9.892	0.68 ± 0.10 (↑ 0.03%)	14.51 ± 0.27 (↓ 2.49%)	5016.57 ± 209.48(↑24.85%)
	15.62	0.67 ± 0.07 (↑ 1.52%)	14.92 ± 0.82 (↑ 0.26%)	4982.20 ± 534.31 (↑24.00%)

As described in Chapter 4.1.2, the PVA web was not as random as the PVAc nanofibers, where Ht was less than 0.1. Overall, the toughening of composites with PVAc electrospun interlayers were superior to those with PVA as the interlayers. Improved toughness resulted from more contact area between fibers and matrix resin. Once imbedded fibers were saturated at optimum basis weight, further toughening was not possible at greater basis weight. In this study, 10 g/m^2 was the optimal basis weight for PVAc interleave. Toughness improved by 25% without any decreases in shear testing.

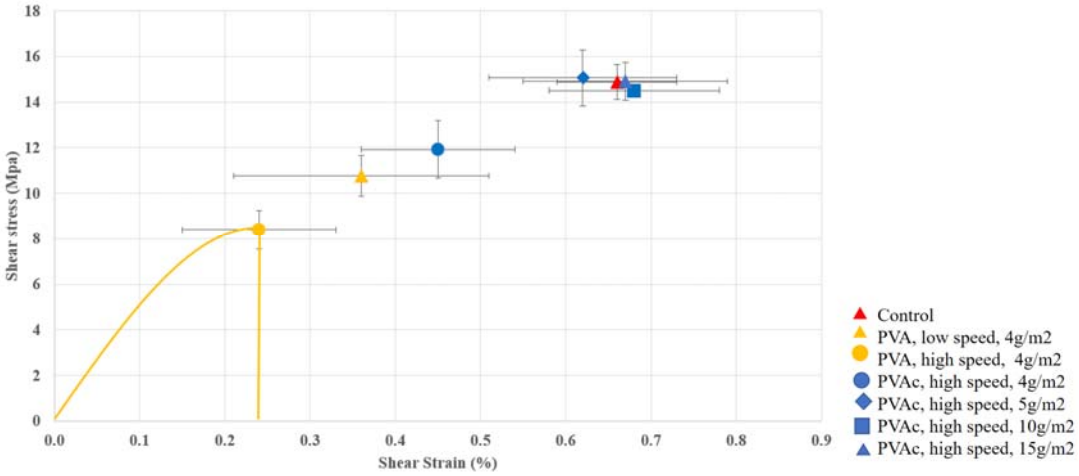

Figure 4.13 Graph of shear test results with different eletrospun interlayer with x axis as shear strain and the y axis as shear stress

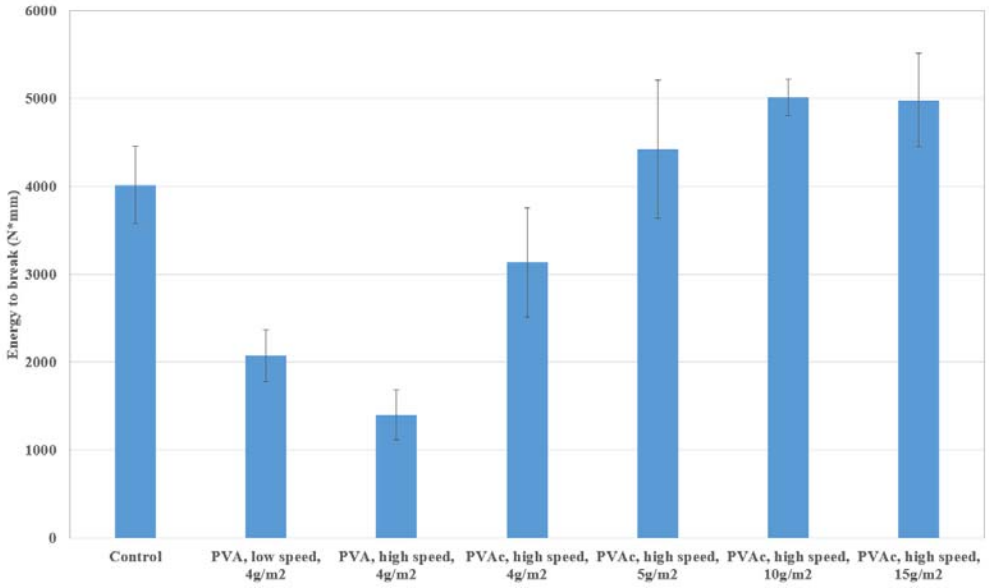

Figure 4.14 The toughness of CFRP with different electrospun interlayers

4.1.7 Morphology of Fracture Surface

Images of the fracture surface were taken with confocal microscopy, Figure 4.15. The fracture surface of the control sample and those CFRPs having electrospun interlayers had quite different morphologies. The control sample failed at the carbon fiber surface, while samples having the electrospun interleave failed in the matrix. Thus, the electrospun interlayers led to cracking in matrix resin opposed to cracking as the carbon fiber surface.

The brittle fracture surface from the control sample is in direct contrast to the ductile fracture modes observed for composites containing PVA and PVAc electrospun interleaves. Among the CFRP having electrospun PVA, the carbon fabric layer peeled off at the matrix rich domain, which led to ductile deformation of matrix resin. CFRPS having electropsun PVAc had shown spatially fragmented portions of matrix polymer were removed from the surface of carbon fiber.

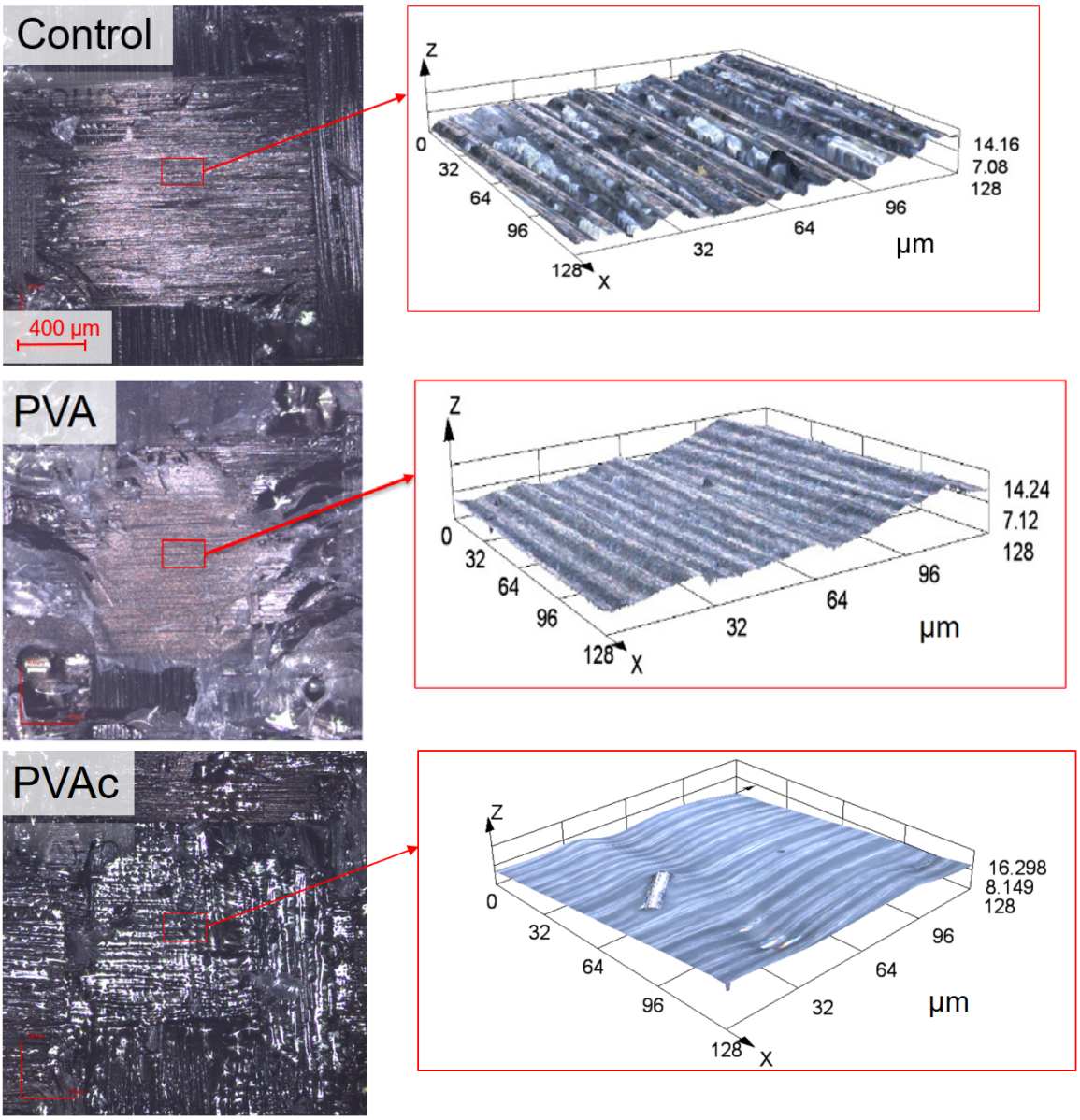

Figure 4.15 Fracture surface images taken from confocal microscopy. From the top to the bottom are fracture surface of control sample, CFRP with electrospun PVA and PVAc interleaves with basis weight as 4 g/m^2. Left: magnification as 5, 2D image. Right: magnification as 100, 3D image.

Morphological differences between fracture surfaces revealed modes of interleave toughening, which distinguished the performance of electrospun PVAc from that of PVA. The ductile deformation of matrix polymer and the ability to keep more matrix resin in tact with carbon fiber led to improved toughness. But, nanofibrous interleaves can also introduce crack in the matrix during fabrication; these cracks can later serve as defects that weaken the composite.

4.1.8 Summaries and Conclusions

Electrospun webs made from PVA and PVAc were integrated into CFRPs as interlayers. Their ability to enhance the delamination resistance and toughness of CFRPs was evaluated. Toughening was affected by the chemistry of the interleave and their basis weight. CFRP containing electrospun 4 g/m^2 PVA demonstrated adversely affected the toughness of composites. Further, oriented fibers and lower basis weight interlayers yield worse performance among CRFRPS. CFRP containing electrospun 4 g/m^2 PVAc did not show a reduction in toughness. Unlike PVA, PVAc is a hydrophobic polymer. At higher basis weights, PVAc interleaves provided more contact area between nanofibers and matrix polymer, which resulted in greater toughness. The optimal basis weight of the PVAc interleave for toughening the CFRP was 10 g/m^2, wherein toughness was improved by 24.85% while the shear load and strain were unchanged (practically the same as the control sample).

Fracture surfaces had revealed modes of reinforcement and failure within CFRPs after shear testing. PVA and PVAc interlayers resulted in ductile fracture surfaces. Reinforcement was characterized by a shift from fracture at the rough matrix/carbon fiber interface to smooth matrix resin along the carbon fiber surface. The fracture surface of

CFRPs containing PVAc interleave underwent greater resin deformation than those containing PVA interleave. As a result, PVAc containing CFRPs exhibited improved toughening.

References

[1] Fong, H., I. Chun, and D. H. Reneker. "Beaded nanofibers formed during electrospinning." *Polymer* 40.16 (1999): 4585-4592.

[2] Ryu, Young Jun, et al. "Transport properties of electrospun nylon 6 nonwoven mats." *European Polymer Journal* 39.9 (2003): 1883-1889.

[3] Deitzel, Joseph M., et al. "The effect of processing variables on the morphology of electrospun nanofibers and textiles." *Polymer* 42.1 (2001): 261-272.

[4] Schmid, Roland. "Recent advances in the description of the structure of water, the hydrophobic effect, and the like-dissolves-like rule." *Highlights in Solute-Solvent Interactions*. Springer Vienna, 2002. 59-90.

[5] Petras, David, et al. "The Effect of PVAc Solution Viscosity on Diameter of PVAc Nanofibres Prepared by Technology of Electrospinning." *AIP Conference Proceedings*. Ed. Martin Zatloukal. Vol. 1375. No. 1. AIP, 2011.

[6] Fennessey, Sian F., and Richard J. Farris. "Fabrication of aligned and molecularly oriented electrospun polyacrylonitrile nanofibers and the mechanical behavior of their twisted yarns." *Polymer* 45.12 (2004): 4217-4225.

[7] Álvarez, Estrella, et al. "Surface tension of organic acids+ water binary mixtures from 20 C to 50 C." *Journal of Chemical & Engineering Data* 42.5 (1997): 957-960.

[8] Baji, Avinash, et al. "Electrospinning of polymer nanofibers: effects on oriented morphology, structures and tensile properties." *Composites science and technology* 70.5 (2010): 703-718.

[9] Li, Zhenyu, and Ce Wang. "Effects of working parameters on electrospinning." *One-dimensional nanostructures*. Springer Berlin Heidelberg, 2013. 15-28.

[10] Bhardwaj, Nandana, and Subhas C. Kundu. "Electrospinning: a fascinating fiber fabrication technique." *Biotechnology advances* 28.3 (2010): 325-347.

[11] Yuan, Xiaoyan, et al. "Morphology of ultrafine polysulfone fibers prepared by electrospinning." *Polymer International* 53.11 (2004): 1704-1710.

[12] Koysuren, Ozcan, and H. Nagehan Koysuren. "Characterization of poly (methyl methacrylate) nanofiber mats by electrospinning process." *Journal of Macromolecular Science, Part A* 53.11 (2016): 691-698.

[13] Reneker, Darrell H., and Alexander L. Yarin. "Electrospinning jets and polymer nanofibers." *Polymer* 49.10 (2008): 2387-2425.

APPENDIX B.Calculation of PVAc Volume

Measurement of solution density,

$$\rho_{88\%PVA} = \frac{\Delta m}{V} = \frac{10.1344g}{10ml} = 1.01134\text{g/ml}$$

$$\rho_{PVAc} = \frac{\Delta m}{V} = \frac{11.039g}{10ml} = 1.1039\text{g/ml}$$

Decision of PVAc volume,

4 ml, 12%, 88% hydrolyzed PVA

$$\mathrm{m}_{solution} = 4ml * \frac{1.0134g}{ml} = 4.0538g$$

$$\mathrm{m}_{88\%\,PVA} = 4.0538g * 12\% = \mathbf{0.4865g}$$

?ml, 40%, PVAc

$$\mathrm{m}_{solution} = \frac{\mathbf{0.4865g}}{40\%} = 1.2162g$$

$$\mathrm{V}_{solution} = \frac{1.2162g}{1.1039g/ml} = 1.1017ml \approx \mathbf{1.1ml}$$